Characterization and Prediction of Fluvial Bank Retreat Using Novel Physical Experiments

Emily Dickson

A Thesis
in the Department of
Geography, Planning and Environment.

Presented in Partial Fulfilment of the Requirements for the
Degree of Master of Science (Geography, Urban and Environmental Studies)
at Concordia University,
Montréal, Québec, Canada

July 2023

CONCORDIA UNIVERSITY

School of Graduate Studies

This is to certify that the thesis prepared

By: Emily Dickson

Entitled: Characterization and Prediction of Fluvial Bank Retreat Using Novel Physical Experiments

and submitted in partial fulfilment of the requirements for the degree of

Master of Science (Geography, Urban and Environmental Studies)

complies with the regulations of the University and meets the accepted standards with respect to originality and quality.

Signed by the final Examining Committee:

_____ External Examiner
Dr. Bruce MacVicar

_____ Examiner & Chair
Dr. Leonard Sklar

_____ Supervisor
Dr. Pascale Biron

_____ Supervisor
Dr. Jay Lacey

Approved by: _____
Dr. Craig Townsend, Chair of Department

_____ 2023 _____
Date Dr. Pascale Sicotte, Dean of Faculty

ABSTRACT

Characterization and Prediction of Fluvial Bank Retreat Using Novel Physical Experiments

Emily Dickson

Understanding sediment transport and bank erosion in rivers has been a key area of active research for many decades. This research project uses a unique new Outdoor Experimental River Facility (OERF) located at the Université de Sherbrooke to run novel experiments to further our fundamental understanding of fluvial bank retreat processes. The experimental river is unique in that its floodplain is considerably larger (50 m by 20 m) than standard laboratory facilities and allows for the channel to freely migrate laterally instead of being constrained by laboratory walls. Three stages of progressively larger upstream disturbances consisting of sandbag perturbations were added to a straight gravel-bed channel to determine if any morphological changes occurred. Using an Acoustic Doppler Velocimeter (ADV), water velocity was measured to quantify the flow field and calculate bank and bed shear stress for four experimental phases: 1) no disturbance, 2) small, 3) medium and 4) large sandbag perturbations. Drone photogrammetry was used to generate digital elevation models (DEMs) to visualize erosion and deposition. Bank shear stress measurements were variable, and more research is needed to determine the optimal sampling techniques. Overall, no meander formation occurred during the experiment, which can be attributed to variables such as river armouring, lack of sediment input, and the time frame of the experiment. This study helps provide an increased understanding of bank erosion which will be useful for future bank stabilization projects related to meandering rivers in Quebec, and globally around the world.

Acknowledgements

I would like to express my sincere gratitude and appreciation to my supervisors Dr. Pascale Biron and Dr. Jay Lacey, whose support, patience and feedback have been incredibly valuable during this journey. I want to express my thanks to André Renault and Basem Mahmoud for their relentless efforts on the field and in the lab to assist my development. The contributions of Dr. Mélanie Trudel and Dr. Leonard Sklar for their ideas and coursework, Nicholas Simard, Daniel Breton, Jason Duguay, and Valérie Dumoulin for their assistance with the OERF, and Guénolé Choné for his technical assistance throughout my program are also acknowledged and appreciated. I want to express my gratitude to all of the undergraduate interns and volunteers who helped with data collecting and analysis, Carolane Bergeron, Imene Ben Nasr, Thibault Buffiere, Marine Bruder, Gabriel Chénard, Toumia Ghribi, Arthur Labrecque, Élisabeth Lapierre, Dencil Mathew, Amal Mzoughi, Bryanna Pilkington, Antoine Pruneau, Sergio Redondo, and Mahmoud Hamdy Aly Abdelbaky. Thanks to the financial assistance provided by the Natural Sciences and Engineering Research Council of Canada (NSERC) (Discovery grants P. Biron, J. Lacey), FRQNT Team grant, Concordia University, GRIL and the Canadian Water Resources Association Ken Thomson Scholarship which allowed me to complete my thesis. And finally, I would like to thank my parents, Anna-Marie and Douglas, my sister Amanda, and my partner Arthur for their unwavering support and encouragement over the last few years.

Table of Contents

List of Figures

List of Tables

1 Introduction

Rivers are intricate systems that have an important impact on the natural landscape and on built environments (Rodriguez-Iturbe et al., 2009). They are essential to many different ecoservices and are responsible for ecosystem health, economic prosperity, and human populations around the world (Anderson et al., 2019). To determine how these river systems function, it is vital to understand the complexity of river systems and the natural and human factors that act upon them.

Human settlements are often built nearby to rivers (Macklin and Lewin, 2019). This proximity allows for easier access to a water supply and more efficient trade and navigation routes (Anderson et al., 2019; Macklin and Lewin, 2019). However, this close proximity between human-made structures and the natural environment can have negative environmental repercussions (Macklin and Lewin, 2019). These negative environmental repercussions can be seen to increase over time, with the process of urbanization gradually moving settlements towards larger cities and megacities (Fang et al., 2018). Anthropogenic impacts on urban rivers include higher runoff rates caused by paved surfaces, as well as changes to natural sediment dynamics (Macklin and Lewin, 2019). Bank erosion and lateral migration of meandering rivers are frequently observed during floods, and result in safety concerns to human settlements, as well as destruction to property. Changes to catchment areas such as channelization and riverbank protection are often utilized to protect urban areas from flooding and erosion, however they are not always successful (Reid and Church et al., 2015, Liu et al., 2017b). There is thus a need for a more complete understanding of erosional processes including planform evolution and meander formation, to help urban planners and river managers anticipate and engineer solutions to bank erosion for public safety.

There are many different ways to study the planform evolution of rivers and to give researchers a more complete understanding of erosional and meandering processes to assist with the management of rivers. This can include collecting velocity data, estimating sediment transport, using drones for photogrammetry and visual interpretation of rivers. These interpretation tools coupled with other numerical and physical analytics of rivers provide a useful snapshot of the functions of rivers.

Studying geomorphological and planform changes such as meander formation is complex in nature and has been previously attempted using small-scale experimental work. This is because experimental river systems allow for controlled small-scale experiments where artificial flow events can be recreated. Laboratory experiments take advantage of precise measuring devices to provide detailed information regarding the dynamics of streams (van Dijk et al., 2013). These experimental facilities, however, have grain size constraints, as they are scaled down, simplified, representations of rivers with narrower and shallower channels than observed in nature. For sediment transport to occur in these flume channels, grain size must be limited in size, usually with coarser particles corresponding to the sand size (< 2 mm) (Peakall et al., 1996). Therefore, flume studies on meanders have so far been limited to sand-bedded environments whereas gravel-bed rivers have been mostly studied in field settings (Carson, 1984; Ferguson, 1987; Church, 2002).

Most laboratory flumes are constrained by laboratory walls, which limits the size and sinuosity of meanders that can be studied (Friedkin, 1945; Schumm and Kahn, 1972; Sahagian et al., 2022). Flumes also normally have shallow depths in order to maintain an adequate width-to-depth ratio (Wilcock et al., 2008). Because the length of indoor flumes is inevitably limited by room dimensions, there are also scaling issues when a channel is too short to initiate meandering downstream (Shuurman et al., 2016). Studying rivers in the field is also difficult, as natural hazards, unsafe working conditions, unpredictable weather conditions, and time scales can make it difficult to collect data in natural rivers. Therefore, there needs to be an intermediate scale that bridges the gap between natural rivers and small-scale flumes to further our understanding of river systems.

My research project aims to fill in these gaps in current knowledge about bank erosion processes by examining erosion at a new large-scale outdoor facility, the Outdoor Experimental River Facility (OERF), located at the Université de Sherbrooke in Quebec (Figure 1). This research will further knowledge about the processes that impact rivers, including erosion and how meanders form, helping people to live more sustainably near rivers and understand more about river systems and erosion.

Figure 1: Birds eye view of the OERF facility at the Université de Sherbrooke.

2 Literature review

2.1 River processes

Riverbank processes including erosion is a natural procedure occurring in all river systems. One of the results of erosion, bank retreat, is generally impacted by a combination of fluvial erosion and mass failure events (Semmad et al., 2021). Although erosion can cause adverse events for infrastructures, it is also an essential process for forming and maintaining natural rivers (Nardi et al., 2013). This process, when undisturbed, can result in dynamic equilibrium, the condition in which steady state of the river has been reached (Bravard et al., 1986; Nardi et al., 2013).

Bank erosion, which contributes to this dynamic equilibrium, is important because it promotes the diversification of habitats and aquatic environments, which can increase the stream biodiversity (Piégay et al., 1997; Florsheim 2008; Choné & Biron 2016). Natural flood events are the most significant drivers of sediment transport and erosion (Leyland et al., 2017). These

flooding events are part of the natural dynamic of river systems and have positive impacts on aquatic ecosystems, which are adapted to large fluctuations in discharge and water levels. In addition to habitat diversification, flooding can replenish nutrients in land ecosystems and rejuvenate soil fertility (Talbot et al., 2018). It is also a valuable process in areas where there are decreasing groundwater and river water levels (Brock et al., 2013) and it helps reconstruct floodplains (Talbot et al., 2018). Despite these benefits, humans may actively work to prevent erosional processes when they have the expectation that rivers should be immobile (Darby et al., 2000). This works against the natural morphodynamic equilibrium of the river, which relies on some level of lateral mobility of the sediments (Darby et al., 2000).

Changing climatic conditions also impact extreme river events, particularly in areas also affected by land use changes such as deforestation or urban sprawl (Panagoulia, 1997; Piégay et al, 1997; Wijeskara et al., 2012). Worldwide there have been increases in flooding events, and there is a high likelihood that this trend will continue (Brock et al., 2013; Famiglietti, 2014; Talbot et al., 2018; Tabari, 2020; Gori et al., 2022), with anticipated growing negative impacts on natural and built environments (Tabari, 2020). Therefore, it is of utmost importance to gather a more thorough understanding of the factors that explain erosion and sediment transport processes to mitigate these negative impacts.

2.1.1 Bank erosion

As mentioned, bank erosion is essential for the creation and progression of channel migration which leads to the long-term evolution of channel pattern and morphology (Florsheim et al., 2008). Several variables influence the extent of bank erosion occurring in rivers, including but not limited to river geometry, bank vegetation and sediment type (Florsheim et al., 2008; Goharrokhi, 2015). For example, river geometry can influence if mass failure events will occur (Goharrokhi, 2015). For vegetation, riparian vegetation stabilizes the bank and reduces the amount of bank erosion occurring, as the roots create more cohesion between the soil particles (Florsheim et al., 2008; Rey, 2009). The vegetation increases the soil shear strength, which is also dependent on sediment type, through root systems that restrict soil particle movement on slopes (Li et al., 2006). The river morphology is largely influenced by the vegetation as there is often increased hydraulic resistance since vegetation decreases local flow velocities. That is, the earliest stages

towards the transformation of sediment deposits into bars, and subsequently into new islands and floodplains, are pioneer plants (Vargas-Luna et al., 2019).

Cohesion force between the sediments is also an important factor in determining the volume of bank erosion occurring. If the shear strength of the upper bank is lower than the gravitational forces, mass failure events (i.e., bank erosion) will occur. These events are often intensified by larger flow events such as flooding (Osman and Thorne, 1998; Rinaldi and Darby, 2007). This is because during high flow events the shear stress on banks increases, and the critical shear stress due to higher flow velocity may be exceeded, thus mobilizing sediments and resulting in erosional processes (Florsheim et al., 2008). Therefore, because of this, there is often a larger amount of bank erosion that occurs in mass flow events.

Bank erosion occurs in highest frequency on the outer bank side of rivers and is a direct result of mass wasting, fluvial processes, undercutting and basal erosion (Hupp and Osterkamp 1996; Duan, 2005; Florsheim et al., 2008). Bank failure often occurs when the bank resistance is less than the gravity which causes the collapse of the banks (Duan, 2005). Basal erosion, defined as the fluvial entrainment of bank material by flow-induced forces that act upon the bank surface including the drag force, resistance force and lift force (Duan, 2005) also has a significant impact on erosion. Deposition will occur if the rate of deposition exceeds the rate of entrainment, and erosion will occur if the opposite is true (Duan, 2005). With flow-induced erosion, the steeper banks will eventually lead to slope instability and cause bank failure (Osman and Thorne, 1998). This is because the toe of the bank is scoured, which removes the sediment lower down the bank and causes the upper part of the bank to collapse (Florsheim et al., 2008). There is a direct relationship between bank retreat, rate of fluvial transportation and the sediment supply caused by erosion. This process is extremely nonuniform and it is therefore difficult to make accurate predictions of long-term erosion rates (Florsheim et al., 2008).

2.1.2 Meandering rivers

Meandering rivers occur in valleys with relatively shallow slopes which also happens to be the ideal locations for many human settlements (Chang, 1984). Thus, there exists a high potential for conflict between meeting human needs in these environments, and the fluvial processes that

occur in this type of channel. Notably, bank erosion is an important factor of meander dynamics, and it is important to have further understanding of it (Braudrick et al., 2009).

Meanders form when water in the river channel erodes sediments on the outer bank and deposits these sediments downstream on the inner curve of the bank, in what is called a point bar (Werner 1951; Lewin 1976; Rhoads and Welford 1991). Rivers that form meanders generally have cohesive floodplain material that add strength to the banks (Kleinhans et al., 2009; van Dijk et al., 2013). Without cohesive material or vegetation, the bank has limited strength, and this can cause the river channel to widen and braid instead of meander (Braudrick et al., 2009; Parker et al., 2011; van Dijk et al., 2013). Another requirement for the formation of meandering rivers is a single threaded-channel without mid-channel bars that can be achieved with moderately low width-to-depth ratios (Shuurman et al., 2016). The width-to-depth ratio is affected by the equilibrium between bank erosion and inner bend accretion rates (Shuurman et al., 2016). This erosion that occurs along one side of the riverbank is balanced by floodplain formation on the opposite side of the channel, which allows the river to maintain its approximate width (van Dijk et al., 2012).

Meandering rivers generally consist of geomorphic units of pools and riffles which appear in regular sequences. Riffles are characterized by high velocities, steeper slopes, coarser bed material and intense turbulent mixing, whereas pools are generally deeper and slower (Kang & Sotiropoulos, 2011). Meanders have three-dimensional flows that consist of secondary (helical) flows, shear layers, vortices, and turbulent stresses, making the formation of meanders complex as there are many variables to consider (Kang & Sotiropoulos, 2011). The curvature-driven and topography-driven secondary flows are the main types of flows seen in a meander (He, 2018). The curvature of a meanders causes centrifugal forces between flow layers, forming the secondary (helical) flow (Stoesser et al., 2010; He, 2018), which are formed through an imbalance of inertial and transverse pressure gradients and move toward the outer curve of the banks (Stoesser et al., 2010; Riesterer et al., 2016).

From an initially straight channel, generally defined as a river with sinuosity of less than 1.5, (Chang, 1984) there are different stages of the evolution, and sinuosity of meandering rivers, starting from stage 1 with the presence of alternating bars (Figure 2). In straight channels alternating bars considerably impact water and sediment movement through the channel (Rhoads and Welford, 1991). This causes the water in a straight channel to shift from straight movement to

increasingly more curved, with the amplitude of this shift increasing further downstream (Knighton, 1998). In stage 2, erosion begins to occur on the opposite side of the banks which increases the curvature of the river (Werner 1951; Lewin 1976; Rhoads and Welford, 1991). In this second stage, incipient pools and riffles begin to form, which is the start of meander formation (Knighton, 1998). Pools and riffles further develop in stage 3, with regular spacing of approximately 5 to 7 channel widths. The final stage is when sinuosity increases and there is the development of meandering channels with riffles at inflection points and pools at bend apices (Knighton, 1998). At this stage, alternating bars are called point bars (Knighton, 1998).

As evidenced above, riverbank erosion is an essential process for the formation of meandering systems (Werner, 1951; Lewin, 1976). For migration of bends to occur, there needs to be bank erosion which is caused by the undercutting of the banks followed by bank retreat from mass failure events (Darby et al., 2007; van Dijk et al., 2013). The eroded bank material protects the banks against further erosion as it reduces the shear stress on the bank by shifting the focus of the high velocity flow (van Dijk et al., 2013). As the bend begins to sharpen, the rate of bend migration begins to increase; this is also impacted by the cohesiveness of the sediments (Kleinhans et al., 2009; van Dijk et al., 2013).

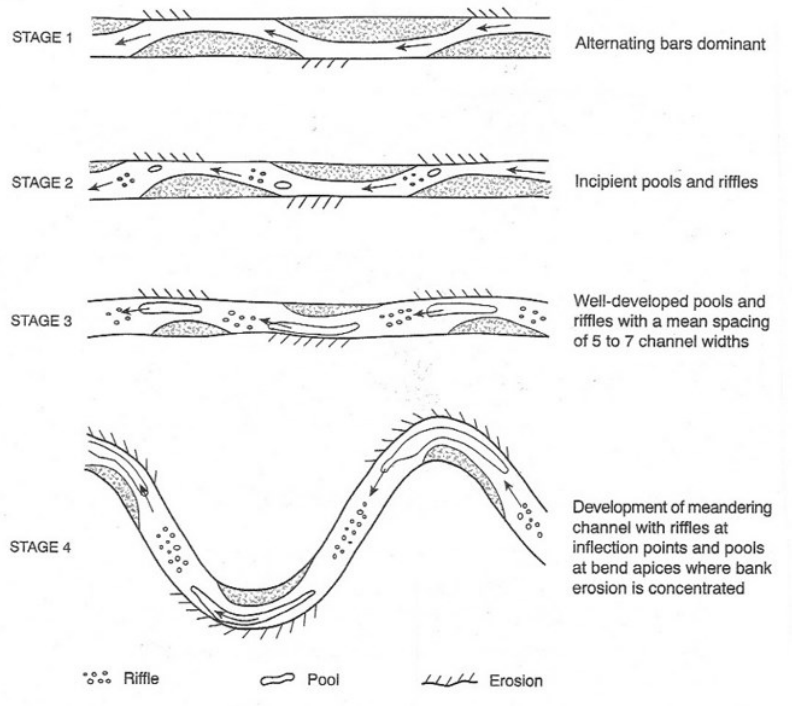

Figure 2: Stages of meandering of a river from a straight channel (Knighton, 1998).

2.1.3 Upstream disturbances for meander initiation

The formation of meandering rivers, as illustrated in Figure 2, generally occurs over long-time scales that are not conducive to field studies. Therefore, the initiation of meandering has primarily been studied using laboratory and numerical experiments where both spatial and temporal scales can be reduced. In laboratory settings, initiating and maintaining meanders from straight streams remains challenging (van Dijk et al., 2013, Sahagian et al., 2022). One issue noted in past laboratory studies is that channels often began to develop bars and planform curves but ended up braiding due to the erosion of weaker outer banks and the accretion on the inner banks (Braudrick et al., 2009).

Early work has shown that oscillations in a straight river channel form meanders following a disturbance in the river systems (Werner, 1951). Several subsequent flume experiments have been successful in demonstrating that to produce river meandering from bank erosion, some sort of continuous inflow perturbations or disturbance is required (van Dijk et al., 2012; Schuurman et al., 2016). This includes water entering at an angle, creating a channel curvature or adding an upstream obstruction or perturbation. There is evidence in a numerical modelling study that free forming meanders can also form without an initial upstream disturbance however this has been hard to achieve in flume studies (Rüther & Olsen, 2007).

Creating an initial channel curvature by manually changing the shape of the initial design has been successful in starting meandering in flume experiments (Shuurman et al., 2016; Sahagian et al., 2022). The channel curvature introduces different flow patterns which cause increased resistance and reduction in slope, thus initiating the start of a meander (Sahagian et al., 2022). An increase in depth also causes the transport capacity to increase where the disturbance is located, which means that the system is no longer stable (Eaton et al., 2006; Kang & Sotiropoulos, 2011). Shear stress remains uniform downstream and lower flow rates typically cause deposition to occur, which initiates the start of new deposition on the opposite side of the channel (Eaton et al., 2006). This creates a positive feedback loop as the change in the flow of water creates a downstream sinuous curve with decreasing magnitude (Eaton et al., 2006; Weisscher et al., 2019; Sahagian et al., 2022).

Of the methods listed above to create meanders, there are several limitations to artificially change the direction of the water flow. One limitation of these methods is that the obstructions

used are not representative of field conditions that occur naturally and are hard to replicate in a natural setting (Sahagian et al., 2022). For example, the instability that causes the formation of meanders is often associated with structures, such as groins, that disrupt the flow (Shuurman et al., 2016, Sahagian et al., 2022). However, such artificial structures do not represent natural field conditions. Overall, it is challenging to replicate nature-based meander forming processes such as large woody debris and natural blocks which divert the flow of water.

2.2 Methods to quantify flow dynamics and measure bank erosion processes

Quantifying bank erosion processes can help predict future bank erosion more precisely and understand the dynamics that cause it. Controlled experiments provide the opportunity to document the flow dynamics that are responsible for bank erosion processes using a variety of methods including ADV (Acoustic Doppler Velocimeter) to measure in situ stream velocities by providing 3D measurements of velocity at high temporal resolution which allows data to be sampled with higher space and time resolution (Palmsten et al., 2015).

Other methods that are used to estimate the bank erosion in river systems include terrestrial LiDAR (Light Detection and Ranging) and drone footage, used to produce repeated Digital Elevation Models (DEMs). The latter technology allows researchers to repeat photos in the same location over a period of time, which provides replicability and the opportunity to visualize where erosion has occurred. Drone imagery can be processed using Structure from Motion (SfM) software that creates 3D imagery from 2D photographs and provides high quality imagery of areas where there have been changes to riverbeds. Thus, this allows for inferences to be made about the amount of morphological change occurring in a fluvial system (Woodget and Austrums, 2017a). This method is particularly useful in areas where there is terrain that is difficult to reach on foot and has the potential to significantly decrease costs associated with field logistics and monitoring (Carrivick and Smith, 2019). It also has the potential to assist with many different processing techniques including change detection, grain size detection and topography (Woodget and Austrums, 2017b; Carrivick and Smith, 2019; Maciel-Pearson et al. 2019). In particular, grain size data mapping is a useful technique for studying fluvial processes and quantifying entrainment, transfer and deposition (Woodget and Austrums, 2017a). SfM methods have made it possible to

observe sediment transport, although larger-scale changes are easier to identify than small-scale ones (Woodget and Austrums, 2017a) as only very high-resolution photographs can be used to delineate individual surface grains (Woodget et al., 2018; Maciel-Pearson et al., 2019). Resolution is dependent on several factors including flight elevation, camera resolution, external shadowing, presence of water and motion blur from wind gusts (Woodget and Austrums, 2017a). Image blur occurs due to the low flying altitudes of drones as well as the effectiveness of camera gimbals and, hence, an appropriate height must be maintained (Woodget et al., 2017a; 2018). Therefore, the accuracy of this method is contingent upon many factors including the resolution of the camera and the grain size that the camera can capture.

2.2.1 Shear stress measurements

Shear stress (τ) is the driving force for sediment transport and is a key parameter needed to predict bank erosion and bend migration (Partheniades, 1965; Sin et al., 2012; Yu et al., 2015). In general, higher bed stress results in an increase in the amount of transported sediments. In order for sediment transport to occur, both friction and gravity needs to be overcome by flow and shear stress to cause sediment movement. Increased slope and increased flow speed will cause the bed shear stress to increase. A higher bed roughness also increases the amount of turbulence occurring which increases the bed shear stress (Yu et al., 2015).

Shear stress, however, is a difficult variable to measure accurately in a river. Several methods are used to estimate shear stress depending on the scale of the experiment (i.e., local versus reach) and the type of velocity measurements available. At the reach scale, the depth-slope product is computed as follows:

$$\tau = \rho g R S \qquad (1)$$

where ρ is water density, g is acceleration due to gravity, R is flow depth and S is channel slope. At the local scale, shear stress can be estimated using the velocity log profile, drag, Reynolds and turbulent kinetic energy (TKE) methods (Biron et al., 2004).

The velocity log profile can be used as one factor that helps determine the amount of sediment transport that occurs (van Rijn, 1984). The flow velocity increases as the height above the bed increases, with the roughness layer estimated as two to five times the roughness height (Figure 3). On rougher bed surfaces the roughness of the rocks may cause some diversion of flow.

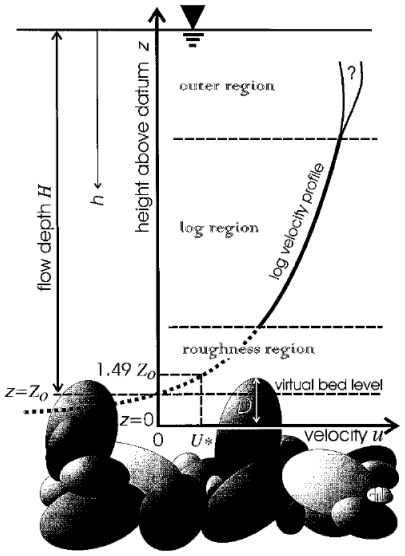

FIG. 1. Illustration of Velocity Profile Extrapolated into Bed and Showing Nomenclature (not to Scale)

Figure 3: Illustration of velocity profile extrapolated into bed and showing nomenclature (not to scale) (from Smart, 1999).

The velocity gradient has a direct impact on bed shear stress and sediment transport. For example, near a large rock, near-zero flow velocity may occur whereas the top of the rock experiences a higher flow velocity (Guo and Zhang, 2016). This creates a difference of pressures, called the Bernoulli effect, where the small amount of pressure on the top of the rock creates fluid forces that allow for sediment transportation (Lucking et al., 2017).

The velocity log profile provides an estimate of the shear velocity (u_*) which is proportional to the slope between velocity and height above the bed and from which shear stress is obtained:

$$\tau = \rho\, u_*^2 \qquad (2)$$

This method requires that a sufficient number of measurements are taken in close proximity to the bed (Biron et al., 1998).

The quadratic stress law relates the average shear stress at the bed to the square of the average fluid velocity (U) using a drag coefficient (C_d) (Williams, 1995), i.e.:

$$\tau = \rho\, C_d\, U^2 \qquad (3)$$

The main challenge with this method is that the drag coefficient is not constant. Shear stress can also be estimated from turbulent fluctuations, for example using the Reynolds shear stress, estimated as:

$$\tau = - \rho < u' w' > \qquad (4)$$

where u' and w' are streamwise and vertical velocity fluctuations, respectively, and $< >$ denotes a time average (Babaeyan-Koopaei et al., 2002; Biron et al. 2004).

The TKE shear stress is also obtained from velocity fluctuations, this time including the lateral component, v', as:

$$\tau = C_1 [0.5 \rho (< u'^2 > + (< v'^2 > + (< w'^2 >)] \qquad (5)$$

where C_1 is a proportionality constant often estimated as 0.19 (Kim et al., 2000).

The TKE method has been shown to be most appropriate in complex flow fields since it is not affected by streamline orientation (Biron et al., 2004).

An ADV can measure turbulent fluctuations in three components and can therefore be used to estimate shear stress using the TKE method. The disadvantage is that since ADVs only measures one point at a time (unlike other velocimeters which collect profiles), it takes time to cover an entire river reach. There is also a need to stabilize the ADV to minimize noise present in the results (Lane et al., 1998). Full turbulence profiles are thus not always possible to collect due to the complex flow of natural rivers as well as the amount of time that it takes to measure. Therefore, the height that the measurements should be taken is important to ensure that it represents the appropriate shear stress, with a non-dimensional height of around 0.1 considered optimal (Biron et al., 2004).

Accurately measuring and quantifying bank shear stress is clearly very important, but most studies so far have focused on bed shear stress, with limited methodological guidance on bank shear stress estimates. Previous studies have shown that shear stresses reach a maximum value on the bed surface and a minimum value at top banks (Chow 1959; Osman and Thorne, 1988; Goharrokhi, 2015). As bed shear stress is not equal to the shear stress on the banks, different measurements need to be taken to appropriately quantify the difference. Bank shear stress has been investigated in the studies of Hooke (1975), Hopkinson and Wynn-Thompson (2016) and Kozarek

et al., (2023). Planform migration of the channel features impact the bank shear stress values and therefore measurements need to be performed across multiple timeframes to increase the replicability of the experiment (Hooke, 1975). When analyzing cross-sections compared with Reynolds stresses, logarithmic methods, and the TKE methods, Hopkinson and Wynn-Thompson (2016) have shown that the TKE method provides more accurate shear stress measurements when the banks have limited amounts of vegetation, and that Reynolds stress and TKE should be used together for vegetated slopes. They also concluded that the logarithmic method did not provide an accurate estimate of shear stress which was the same findings as Kozarek et al., (2023) who found that the logarithmic curve and time averaged velocity did not follow a logarithmic profile near sloping banks. In all, there remains a scarcity of studies on the appropriate sampling design for bank shear stress, including the distance to the bank to sample for ADV measurements, and the sampling techniques.

2.2.2 Sediment transport in gravel bedded rivers

Sediment transport is mostly defined between three types of transport, suspended sediment, wash load and bed load (van Rijn, 1984). Suspended sediment is predominantly comprised of clay, silt and fine sand (<0.063 mm) (United States Environmental Protection Agency, 2003) whereas washload is finer than bed load material and remains in suspension at all times (Biedenharn, 2006) and bed load consists of coarser sediments that are too heavy to be suspended in the water column (Brown, 2008).

For sediment transport to occur it is crucial to take into account how lift forces affect sediment transport in comparison to gravitational force, which happens when bed shear velocity exceeds fall velocity (van Rijn, 1984). This is impacted by many factors including the mobility of sediments on a bed and the degree to which a river is armoured. In gravel-bedded rivers, coarser armoured sediment layers are regularly observed (Whiting and King, 2003). Armoured rivers occur when the size of the sediments is larger than the ability of the river to transport these sediments (Whiting and King, 2003). As the river armours the amount of shear stress required to move the sediments greatly increases (Whiting and King, 2003). The smaller sediments are winnowed from the bed and the surface size distribution is truncated, meaning that the flow is only able to transport a certain subset of the initial sediment size distribution. As this occurs more shear stress is required to move the larger sediments that have armoured on the bed.

3 Research question and hypothesis

The OERF provides a unique opportunity to further the understanding of river systems using a real-world scale flume to answer additional questions regarding the evolution and functions of rivers. Therefore, the research questions for my thesis proposal are:

1. What is the planform evolution of an initially straight gravel-bed experimental river following an upstream disturbance?

Further to this question, the sub-questions will also be asked to understand more about the system as a whole:

2. How will changing the size of an upstream disturbance impact the downstream planform evolution?
3. What will be the timescale of geomorphological changes (if any) following an upstream disturbance?

The study aims to fulfil the following three goals:

1. Perform novel physical experiments to better understand bank erosion processes in a large-scale laboratory setting (i.e., OERF) and to apply the gained knowledge to real world scenarios.
2. Quantify the formation of meanders (if any) and planform evolution of an initially straight river.
3. Provide the framework to perform future experiments on the OERF to research bank stabilization techniques.

The first hypothesis is that adding a sandbag perturbation to the experimental river will affect the shear stress and velocity patterns compared to a straight river channel. It is also hypothesized that the impact on these parameters will be observed at the outer bank as the perturbation increases in size. To test these hypotheses and understand spatial variation between zones located upstream, midstream and downstream of the perturbation, detailed ADV measurements will be taken at different cross-sections and throughout different perturbation phases.

The second hypothesis is that once the river reaches equilibrium there will be little transportation of sediment in the straight river channel. Following the construction of the initial perturbation, it is hypothesized that there will be increased erosion on the side opposite the sandbag perturbation and this eroded sediment will be transported downstream. Finally, it is hypothesized that the addition of a sandbag perturbation will cause geomorphological changes to the shape of the river. To test these two hypotheses, drone footage will be taken between phases to assess if any geomorphological changes occur.

4 Methods

4.1 Experimental design

This research was conducted at the Outdoor Experimental River Facility (OERF). The OERF is a 50-m-long by 20-m-wide floodplain that is built on a slope of 0.005 with a maximum discharge capacity of the river being 0.75 m^3/s. Average flow depth for this maximum discharge was 0.25 m, resulting in an average bed shear stress (equation 1) of 12.3 N/m^2. The water is pumped through the head basin, making its way into the experimental river after passing through a sharp crested weir (Figure 4). At the downstream portion of the river a sluice gate controls flow discharge into the downstream reservoir. As the OERF is a brand-new facility, initial experiments and calculations were conducted during the period between May 2021 - November 2021, including the creation of the river channel, with the experimental runs using an upstream perturbation starting in May 2022.

4.1.1 Channel geometry

Migration of bars have been observed in channels where the width-to-depth ratio is large enough for the promotion of meander development (Leopold and Wolman, 1957). Therefore, a width-to-depth ratio of 12 was chosen for the OERF to obtain a geometry that represents gravel-bedded rivers and the associated floodplain (Leopold and Wolman, 1957). As river patterns change depending on width, flow rate, slope, grain size and sediment supply, the goal of the OERF was to

create a river that meandered instead of braided (Leopold and Wolman, 1957) and thus specific geometry was calculated based on this goal.

To determine the channel geometry of a meandering river, the transport stage (TS), which is the optimal minimum value needed for sediment transportation, was calculated based on the sediment size of the OERF. This was calculated with the following formula (Bagnold, 1966):

$$TS = \tau* / \tau*_{\text{critical}} \qquad (5)$$

where $\tau*_{critical}$ is the dimensionless critical shear stress (0.045) and τ^* is the dimensionless shear stress computed as:

$$\tau* = \tau / (\rho_s - \rho)\, g\, D \qquad (6)$$

where ρ_s is the sediment density (kg/m^3), and D is the median diameter (D_{50}) value (in m).

An optimal transport stage greater than 1.2 (above low to moderate transportation) was chosen in combination with the width to depth ratio (Bagnold, 1966; Ceccheto, 2018). For simplification, the initial calculations were based on a rectangular channel which was converted to a simple trapezoidal shape. The channel geometry was initially calculated at 75% of the maximum discharge to ensure there was room for error in case there were miscalculations based on the theoretical numbers.

The optimum depth of the river was calculated to be 0.25 m, with a width of 2.5 m at the base and 3.7 m at the water height. The channel width was built at 0.1 m higher than calculated with a value of 3.9 m to account for any errors from the discharge of the pumps. The bank angle was built at 25.6° (or 2:1) (Figure 4) to ensure that there would not be immediate bank collapse and that bank stability would be maintained. The channel was dug with an excavator and a mold made from plywood was built to check the accuracy of the channel. It was determined that the accuracy was within 0.025 m.

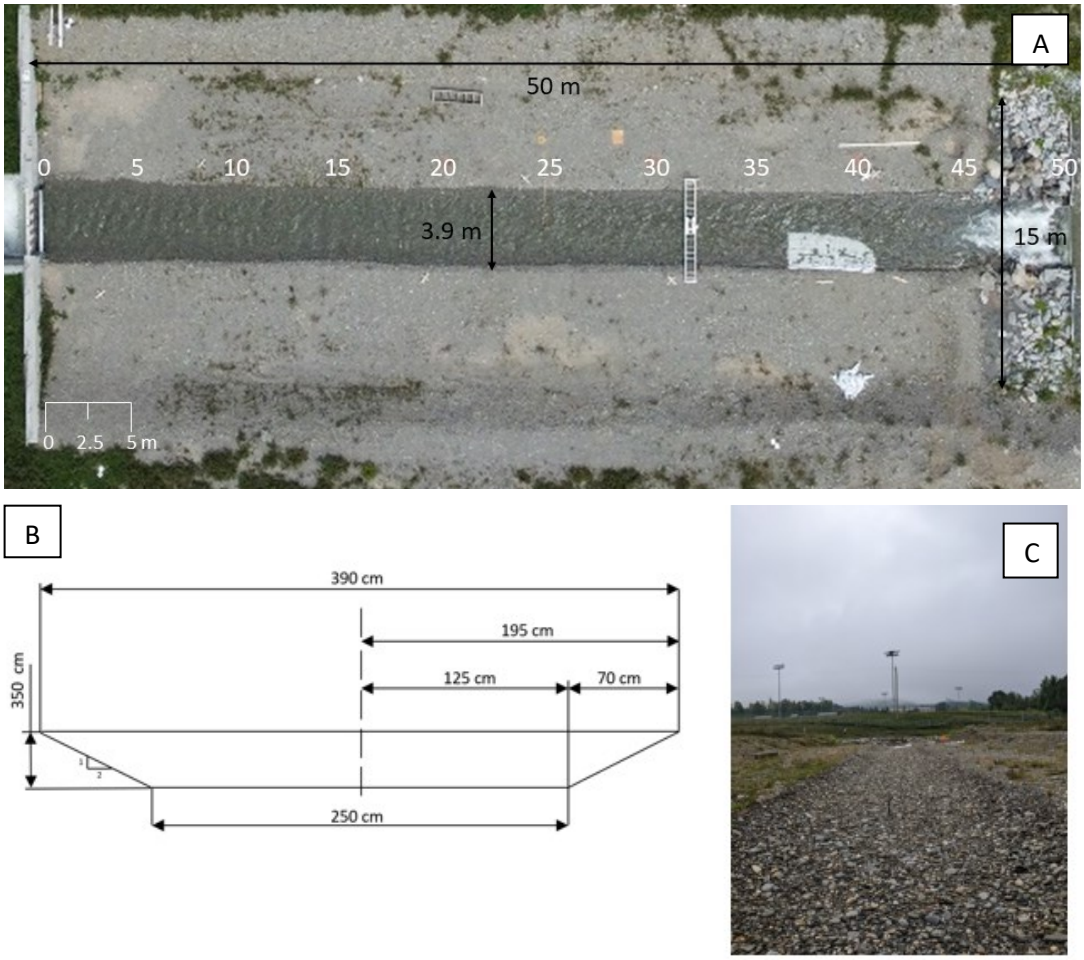

Figure 4: (A) Facility; (B) Channel measurements. Image created by André Renault 2021-07-01 (Renault, 2021); (C) view of river from downstream to upstream.

4.1.2 Channel sediment and sediment transport

The OERF is composed of sediments that include both sand and gravel. The sediment size ranged from 0.08 mm (very fine sand) to 80 mm (fine cobble gravel). For sediment distribution a D_{50} of 10 mm was modelled after Oak Creek from the Parker and Klingeman (1984) study and corresponds to a gravelbed stream. Assuming a dimensionless critical shear stress of 0.045, the critical shear stress to mobilize this grain size is 7.1 N/m^2, so less than the slope-depth average shear stress of 12.3 N/m^2. The D_{84}, where 84% of the particles are smaller than that value, was 34 mm (Figure 5).

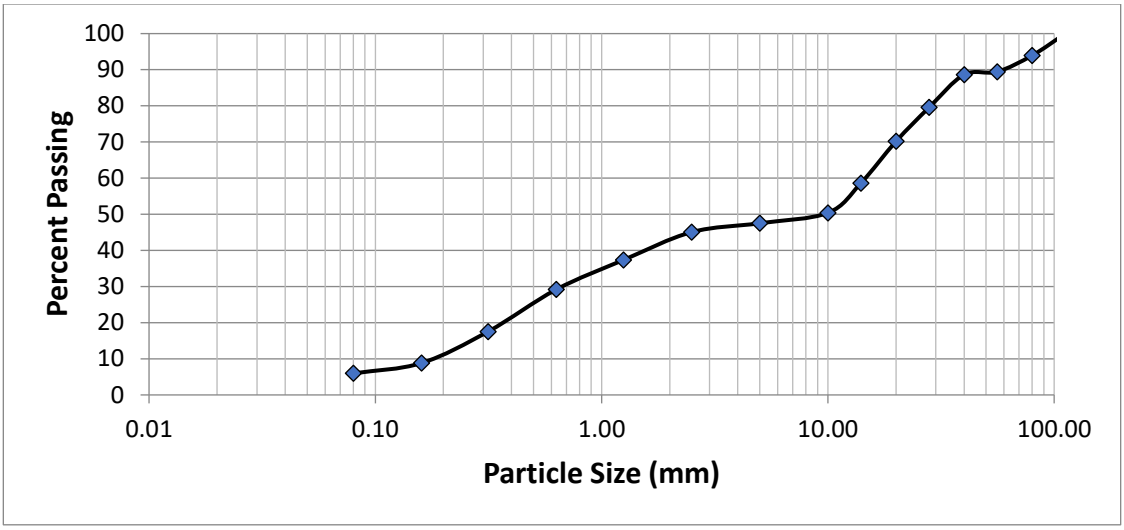

Figure 5: Grain size distribution curve for the OERF.

In order to estimate the rate of sediment transport the Wilcock and Crowe (2003) equation was used. It is designed for mixed-size sediment (poorly sorted) rivers containing both sand and gravel, which corresponds well to the grain size distribution at OERF (Figure 5). There is always a large uncertainty with bedload equations, but it provides a rough estimate of the anticipated amount of sediment transport. The Wilcock and Crowe (2003) equation is as follows:

$$W_i* = f(\tau/\tau_{ri}) \qquad (7)$$

Where τ = bed shear stress, τ_{ri} is the reference shear stress of the size fraction i and W_i* is the dimensionless sediment transport rate of size fraction i defined by the following equation:

$$W_i* = (s-1)\, g\, q_{ib}\, (F_i\, u^{*3}) \qquad (8)$$

Where s = ratio of sediment to water density, q_{ib} = volumetric transport rate per unit width of size i, F_i=proportion of size i on the bed surface and u^* is the shear velocity.

The hiding function equation was added as follows:

$$\tau_{ri}/\tau_{rs50} = (D_i/D_{s50})^b \qquad (9)$$

where the value of the exponent b is derived from the reference shear stress for each size fraction (Wilcock and Crowe, 2003):

$$b=0.67/1+exp(1.5-D_i/D_{sm}) \quad (10)$$

The equation provides a rough estimate of how much sediment transport is expected to occur in the experimental river. A sediment recirculation system is currently being planned to ensure that sediments deposited downstream can be recirculated upstream.

4.1.3 First river trials

The first trials of the river were started on low flow to flush out sediments loosened from construction. The discharge was gradually increased until the full flow value of 0.72 m^3/s to understand more about the behaviour of the experimental river. After a large amount of the fine sediments were washed away, sediment traps were placed mid-stream at 22.5 m (Figure 6). The sediment bins were placed flush with the bottom of the river to collect sediments that were being transported as bedload. The sediment traps consisted of a small wooden frame that was attached to the riverbed with rebar and was used to prevent sediments from collapsing into the trap when the bins are removed (Figure 6). A thin layer of mesh was placed on top of the bins to collect smaller grain sizes (<2mm). Six bins were placed across the width of the river and were rotated when they become full of sediments. Using these sediment traps, a greater understanding of what size and volume of sediment transported was gained for future experiments (Figure 6). A final experiment involving adding painted rocks to the river at approximately 3 kg per minute was conducted to further understand sediment transport processes and determine the distance that different sized sediments could travel. Additionally, some of the sediments were painted orange in order to track the distance they travelled. This provided base information to assess if our initial calculations on sediment transportation were correct and will help estimate the future amounts of sediment that are needed to be added to the river.

Figure 6: Sediment traps that added to the first trial of the rivers in June 2021 (located at 22.5 from upstream). Traps were removed for the second set of experiments.

4.2 Flow dynamics linked to upstream perturbation

4.2.1 Upstream perturbation experiments

Starting in May 2022, the river was run to ensure that it was in equilibrium after being turned off for the winter season. This included running the river at full discharge for the maximum time (approximately 8 hours a day) at 0.72 m^3/s, which results in an average velocity of approximately 1.12 m/s based on a cross-sectional area of 0.8 m^2. Pumps and equipment were tested to ensure the river was ready for experiments by June.

There was no sediment recirculation system available at OERF at the time the experiments were carried out (there should be one in place by 2024), which resulted in armouring of the bed. Armouring occurs when the finer sediments are washed away and cause the riverbed to be rearranged (Sieben, 1999; Pirkhoffer et al., 2021). It was seen that during the first trials the bed surface exhibited the initial phases of armouring and was further armoured in subsequent trials which limited the movement of sand.

Since the initial experiments resulted in only very minor morphological changes, it was determined that a perturbation needed to be added to the river to try to force morphological evolution towards a meandering pattern. The perturbation design was researched and created by Basem Mahmoud, a PhD candidate at the Université de Sherbrooke (Civil Engineering). The goal

of the perturbations was to (1), cause morphological changes to the bed, (2) be based on theory and literature, and (3) be repeatable (Mahmoud, 2022b). The design and MATLAB code was based on previous work by Redolfi et al., (2020) and designed to be scaled to the OERF river. It was modified by Mahmoud (2022b) to include multiple phases, and amplitudes of each Fourier components (harmonics) as shown:

$$\eta(x,y) = \sum_{m=0}^{\infty}\sum_{n=0}^{\infty}|A_{nm}|\,cos\left(\frac{\pi m y}{W}\right)cos\left(\frac{2\pi n x}{L}+\phi_{nm}\right) \qquad (11)$$

where η is bed elevation, x is the longitudinal coordinate, y is the transverse coordinate, Anm and ϕnm are the amplitude and phase of each Fourier components (harmonics), n and m are the longitudinal and transverse modes of the harmonic component, W is the channel width, L is the bar wavelength (Mahmoud, 2022b). From an original straight channel (phase 0), three upstream bar and pool designs were defined using this equation, namely phase 1, phase 2 and phase 3 (Figure 7).

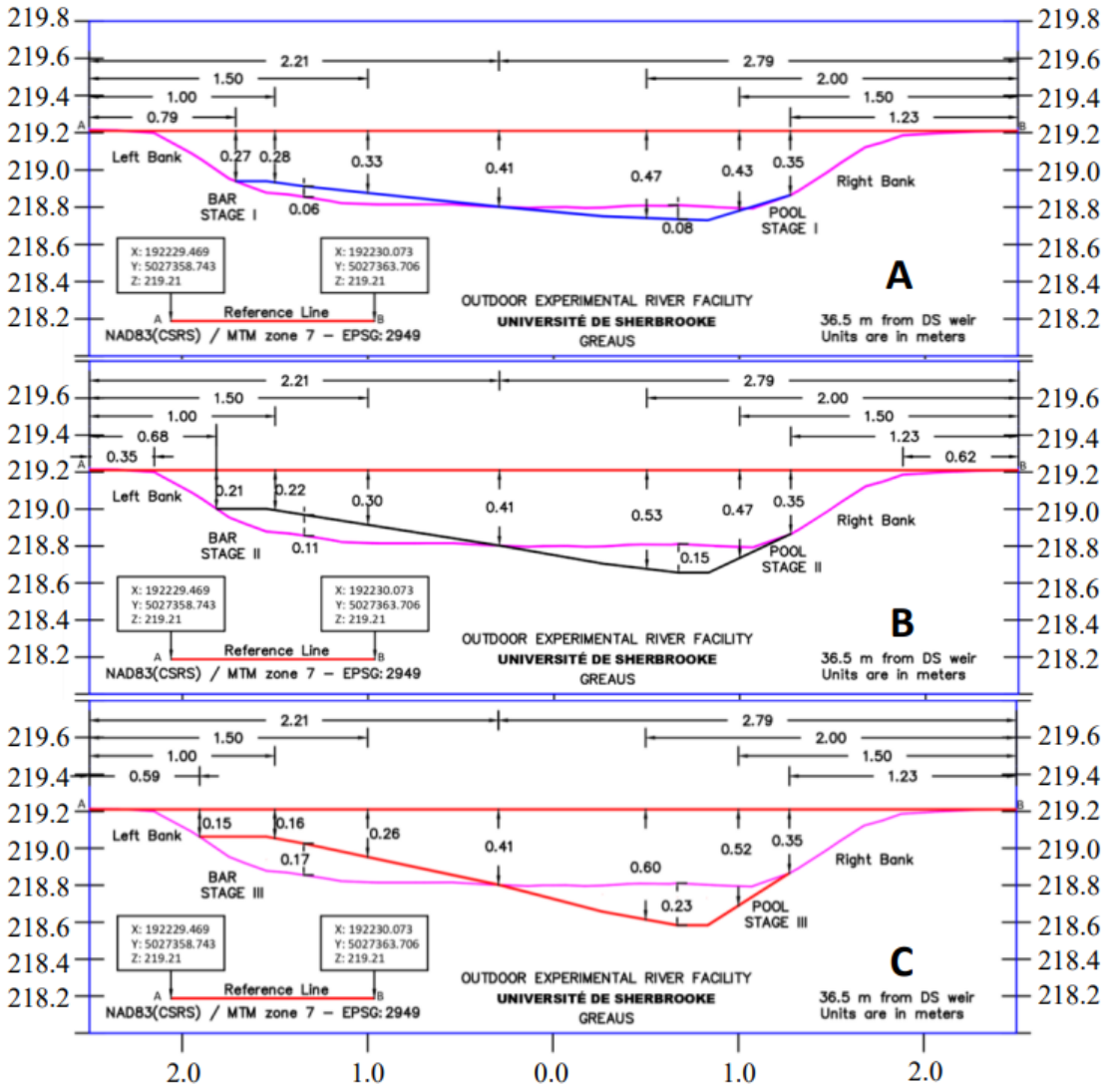

Figure 7: Design specification for the three phases of bar and pool design. Phase 1 (A); phase 2 (B); phase 3 (C). From Mahmoud (2022b).

The initial channel (phase 0) was built in 2021 and re-evaluated starting on May 18, 2022. Phase 1 was built on July 28, 2022, followed by phase 2 (built on August 5, 2022) and phase 3 (built on August 22, 2022). Figure 8 illustrates the differences in size between the small (phase 1), medium (phase 2) and large (phase 3) perturbations. For all phases, the perturbations were shaped by filling sandbags with sediments less than 10 mm, although the sandbags were mostly composed of sand. The length and width of the perturbation remained the same between phases with only the height increasing from phase 1 to phase 3. The sandbag perturbation started 4 m from the rock weir and ended 13.5 m from the rock weir, for a total length of 4 m. The perturbation was a half

tear dropped shape, so the width varied with the widest point reaching half the width of the channel. For each stage an equal sized pool was dug out on the opposite bank. In theory, by creating both the incipient bar and the incipient pool there would be a vorticity imposed on the flow which should drive bank erosion and channel evolution (Schwartz et al., 2015; Tokyay & Sinha, 2020). The conveyance area of the river was kept approximately constant to reduce the amount of constriction occurring and reduce the water surface slope upstream.

An incremental approach was followed for the construction of the perturbation. This allowed us to determine if any morphological changes occurred at earlier phases, as well as the duration that these changes occurred for. Phase 0 was run throughout the summer of 2021 and rerun in 2022 for 50.4 hours to ensure armouring of the bed occurred. Phase 1 was run for 15.0 hours, phase 2 was run for 27.8 hours, and phase 3 for 204.8 hours. Phase 3 did not armour before the end of the experimental period and changes were still occurring at the end of the experiment. All phases were documented to determine the response of the river to the different perturbation sizes, including ADV measurements and drone footage, which will be discussed below.

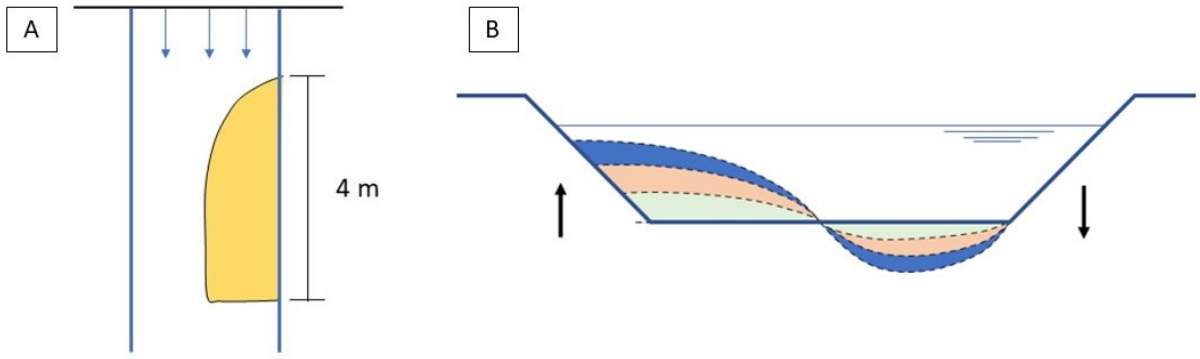

Figure 8: Birds eye view (A) and cross-sectional (B) an of upstream perturbation of the three sizes of pools and bars. From Mahmoud (2022a).

4.2.2 Velocity measurements and shear stress estimates

Following the implementation of each phase, 3D velocity measurements were collected with an ADV near the bank to estimate shear stress and velocity with a variety of methods (Babaeyan-Koopaei et al., 2002, Biron et al., 2004). A 4-m ladder was placed across the river with a retrofitted mount that allowed the ADV to move horizontally across the river, and vertically towards the riverbed (Figure 9a). As it was difficult to measure the precise distance from upstream

due to the rock weir, distance measurements were (unconventionally) stated from the downstream weir. For phase 0, three cross-sections were arbitrarily chosen based on the planned location of the phase 1 perturbation. These cross-sections were measured at 41 m (upstream of the perturbation, hereafter called UPP), 37 m (lower perturbation, LOWP) and 32 m (downstream of the perturbation, DOWN) (Figure 9b). Following the construction of phase 1, it was determined based on visual observations of the river flow that a fourth cross-section at 39 m (in the middle of the perturbation, hereafter called MIDP) should be added (Figure 9b).

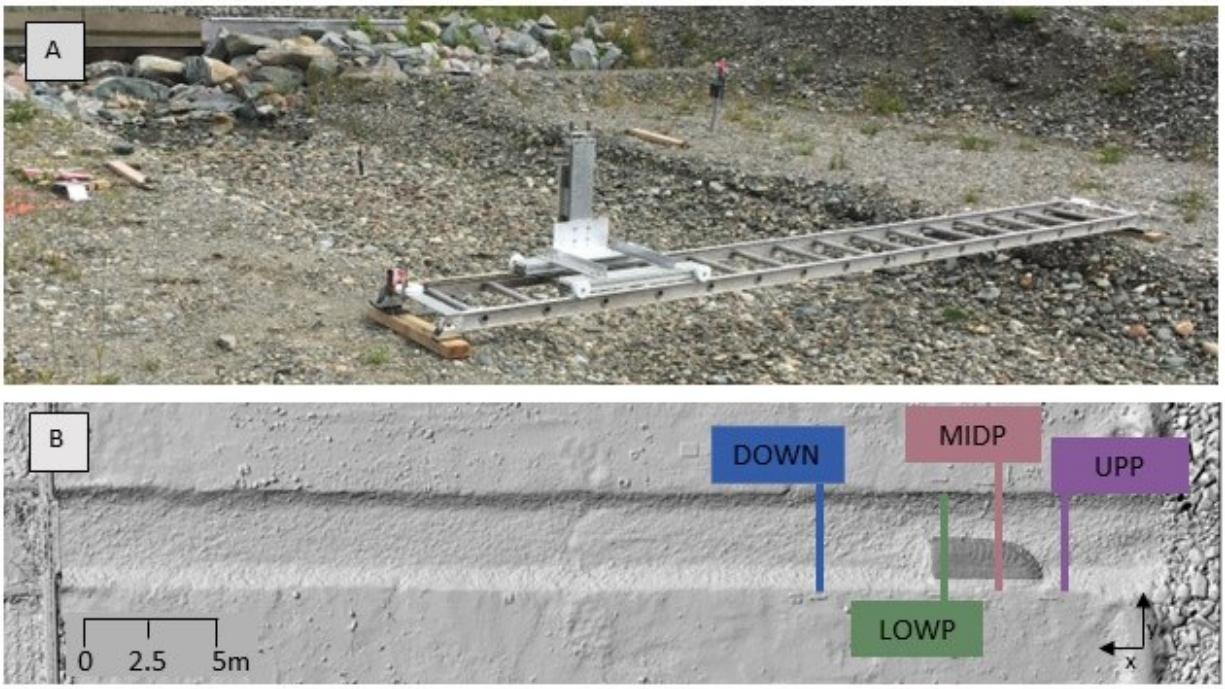

Figure 9: A) Ladder and ADV mount used to measure the ADV data points, and b) Diagram showing where the four cross-sections, 41 m (upstream of the perturbation, UPP), 39 m (upper perturbation, MIDP), 37 m (lower perturbation, LOWP), & 32 m (downstream of the perturbation, DOWN) were measured. Flow direction is from right to left.

As was mentioned earlier, few studies have taken detailed shear stress measurements close to mobile banks. In order to gather ADV measurements in close enough proximity to the bed and bank to estimate shear stress and to provide comprehensive data on flow dynamics in these zones, a grid was developed (Figure 10). Throughout the phases, the grid's design was slightly modified to add points where needed.

The ADV data points were sampled on the same grid for each cross-section. The rows were positioned at 2.5 cm, 5.0 cm, 7.5 cm, 10 cm, 15 cm, and 20 cm above the bed for the near-bank

shear stress. For each row, the ADV data points were measured at 2.5 cm, 5.0 cm, 7.5 cm, 10 cm, 15 cm, and 20 cm from the bank. Three columns were measured for bed shear stress at distances of 100 cm, 140 cm, and 180 cm from the banks. At each column ADV data points were measured at 2.5 cm, 4.0 cm, 6.0 cm, 10 cm and 15 cm from the bed (Figure 10).

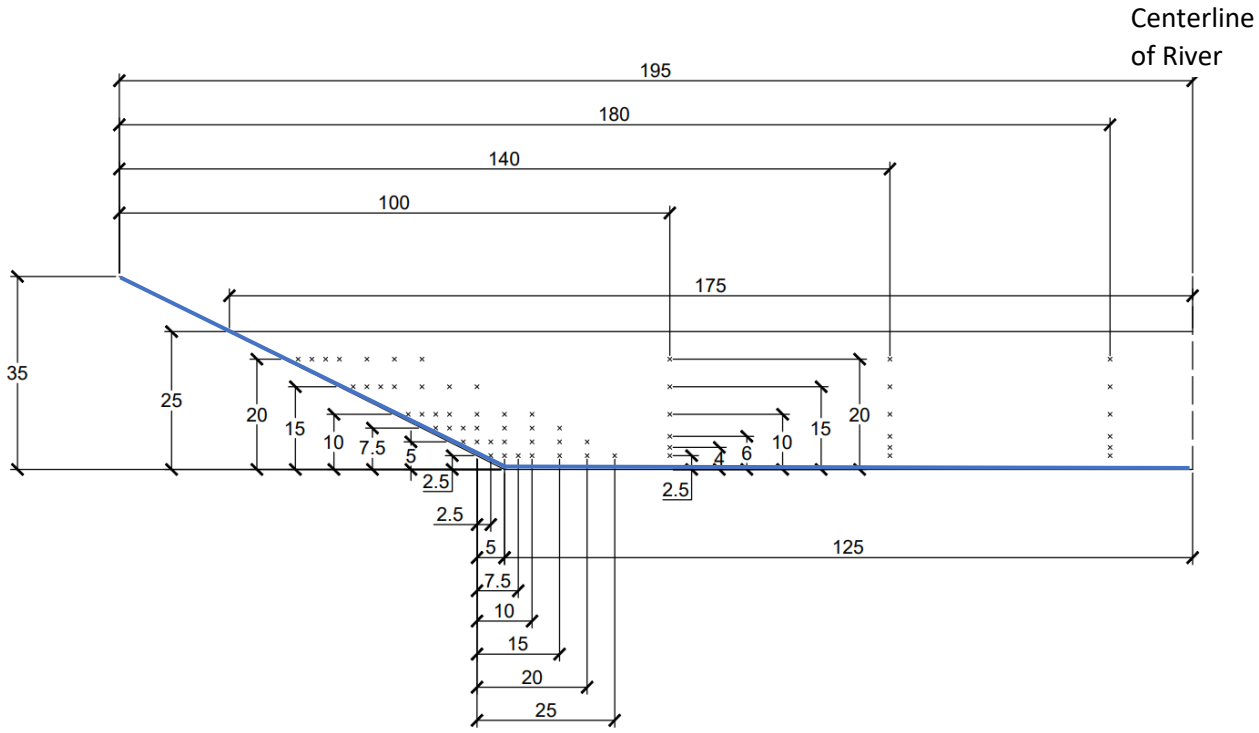

Figure 10: Grid for ADV measurements. Note: The y 7.5 cm and 20.0 cm were not taken for all cross-sections. Image produced by André Renault 2023 (Renault, 2023). Dimensions are in cm. Image is to scale.

The ADV data points were recorded at 50 Hz for a duration of 120s. The velocity sensitivity range was determined based on observed measurements. In general, near-bank measurements were taken at ± 1.0 m s^{-1}, and then increased to ±2.5 m s^{-1} approximately 10 cm from the banks. Occasionally when there was significant spiking the sensitivity range was increased to ±4.0 m s^{-1}, although these points were mostly removed during post processing. In order to reduce the potential of morphological changes affecting the ADV measurements, it was attempted to measure the four cross-sections in the least amount of time possible. However, it was only possible to measure a maximum of two cross-sections per day, and only one cross-section per day for phase 3 due to limited resources. Therefore, the ADV measurements of each phase were collected after the river ran for the same amount of time in order to provide a direct cross-section comparison.

During the summer of 2022, chara algae were found in the downstream reservoirs and a large amount of filamentous algae were found in the upstream basin during sampling (Figure 11). As the chara algae was affixed to the reservoir bottoms, it had no effect on the measurements. The filamentous algae, however, had a large negative influence on the tests at the OERF since it soon overflowed the sediment traps and wrapped around the ADV while measurements were being taken. To decrease the impact of the algae on the measurements, a fence with a fine mesh (1 cm x 1 cm) was constructed upstream of the river to allow water to still move through the system but reduce the algae that entered the river. The fence was built far enough away from the entrance of the river to ensure that flow velocity was not impacted, which was confirmed with pre- and post-velocity measurements. The screen greatly reduced the amount of filamentous algae in the sampling part of the river, however it was unable to completely eliminate it. Therefore, the ADV was washed off in between measurements to remove any algae that got caught.

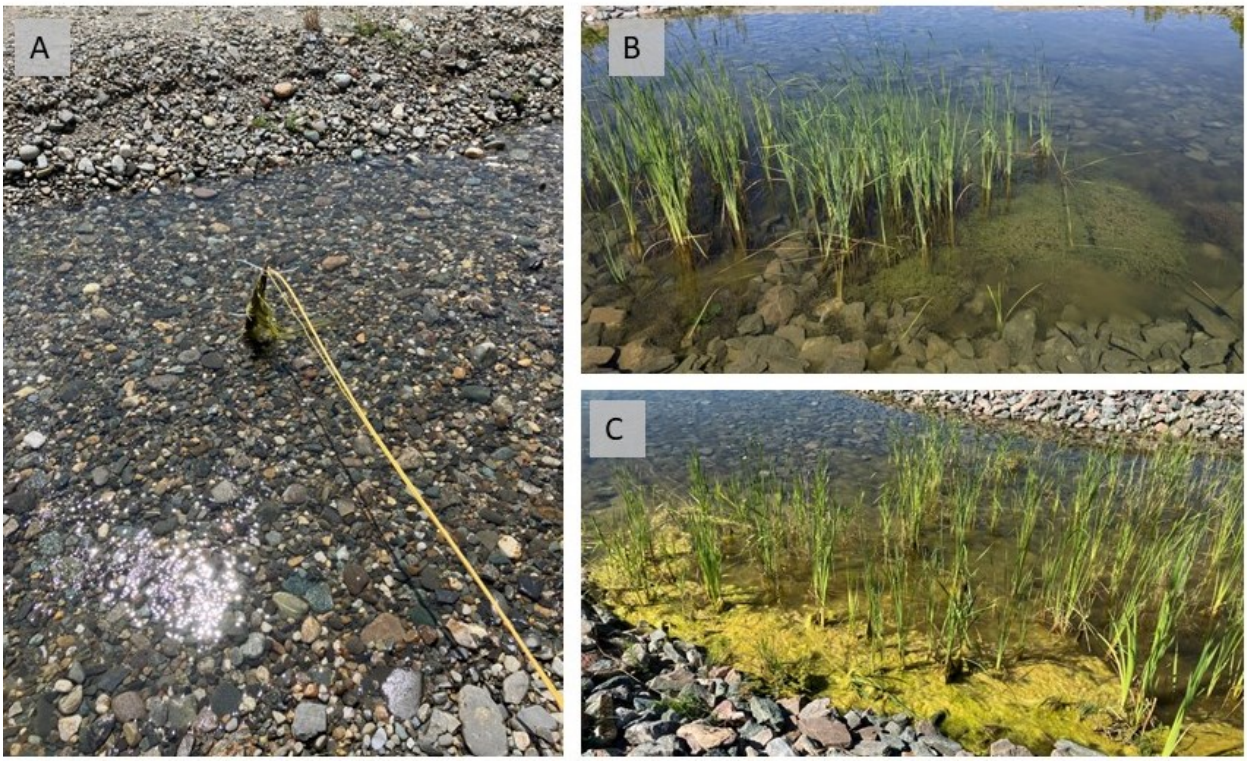

Figure 11: A) Filamentous algae wrapped around the pressure transducers; B) Chara and filamentous algae upstream of the river; and C) Large quantity of filamentous algae upstream of the river.

4.2.3 ADV data processing

To reduce any initial noise, the ADV data was processed with WinADV which uses a de-spiking filter to remove some noise (Bureau of Reclamation's Water Resources Research Laboratory, 1996). The data was then thoroughly examined to eliminate any suspicious data, such as velocity measurements larger than 180 cm/s, which was far above the average data range and far outside the range of the other data points. Investigation into these revealed issues with missing w or v velocity components, and these data points were removed. Additionally, time series of each ADV point was scrutinised to check for any anomalies, specifically for data points with velocity ranges outside of the typical range. Heat maps were also created to look at the overall pattern of data and investigate any extreme outliers. Lastly, power spectra for each of the remaining data points were examined in MATLAB to look for any suspicious time series and eliminate points if they showed a flat power spectra, low correlation, or very high variance across the three velocity components. It should be noted that earlier research has shown that consistent average velocities can still be achieved even when correlation values are as low as 40 % (Martin et al., 2002). This is provided that the sampling length of time is long enough to take an average of more than 60 seconds. For the ADV measurements at the OERF, a sampling interval of 120 seconds was employed, and thus if all other tests and variables were successful, ADV data points with correlation values above 60 % were often kept. If all other variables were excellent, data points with correlation values between 50 % and 60 % were also kept; otherwise, if the other variables were bad, they were eliminated.

Most data points that were removed from the ADV analysis were located near the bed and bank. To guarantee that the results adhered to a pre-set grid, the ADV was mounted on a stationary pulley system. As a result, the placement of ADV data points could not be changed. This meant that some data points were not collected in the most optimal places. This was particularly evident at the near bed and bank locations, as there was more noise in the data due to the presence of large rock when compared to data points taken further from the bed and the bank. The ADV results and, consequently, the shear stress estimations may have been affected by turbulence around larger particles.

Due to the presence of filamentous algae that frequently got caught on the ADV during sampling, several measurements had to be repeated after cleaning off the algae. It is highly likely

that some ADV measurements still had algae on the measuring equipment, affecting the quality of the signal. This is one of the sources of error that is present in the data.

Following the elimination of problematic ADV samples, velocity patterns were examined by comparing phases and cross-sections. The planar (UV) near-bank velocity vectors were calculated for all four phases and cross-sections at a height of 15 cm above the bed. For each cross-section, secondary flow (VW) vectors were also computed. Velocity magnitudes were interpolated using spline (with tension) in GIS (ArcGIS).

Bed and bank shear stress was computed using the different methods. Equation 5 and 3 were used to compute TKE (at points within 0.1 of the flow height) and Reynolds shear stress (based on the projection of the graph) for all midstream bed points. Shear stress was also estimated using the quadratic law based on the drag coefficient (equation 4) and the log profile (equation 2). The three midstream positions were than averaged together (100 cm, 140 cm and 180 cm). For bank shear stress, as it is difficult to quantity what constitutes the 'height of water', the first four points (within 10 cm of the banks) were used for the calculations. To calculate the logarithmic profile for the 'height of water', the nearest distance to the banks were calculated using similar triangles (2:1 angle) to best estimate the 'perpendicular' line to the banks. In addition, a series of ADV data points that were actually perpendicular to the bank were taken to compare the results of the grid ADV points to the perpendicular points. As the nearest distance and perpendicular line gave significantly different shear stress values, and not normal log profiles, it was determined that the log law varied too much to be used with confidence. Furthering this, since the near bank measurements did not follow the logarithmic profile, it was difficult to calculate shear stress using logarithmic curves and time averaged shear stress.

Finally, statistics were calculated to determine if any of the results were significant. As both the bed and bank shear results were nonparametric and assumptions of normality and homoscedasticity were not met, the Kruskal Wallace test was used to test significance. A further multiple comparison Kruskal Wallace test was used to test for specific difference between phases and cross-sections (Siegel and Castellan, 1988).

4.3 Drone and visual observations

4.3.1 Visual observations

Visual observations were completed pre- and post- river run. These observations included a walkthrough of the entire experimental river to note any changes that occurred. Manual photographs and videos of the bed and bank were taken by camera and drone and compared at every phase.

4.3.2 Digital Elevation Models and visually observed erosion

Drone footage using a DJI Mavic 2 Pro was taken at elevations of 30 m, 20 m, 15 m and 10 m to determine the best spatial resolution. Based on these initial tests, it was determined that the drone would be flown at elevations of 30 m and 10 m as they gave the best results. Once the water was drained at the end of each phase, drone footage was used to produce DEMs (Digital Elevation Models) using SfM (Structure for Motion) software (Pix4D).

The drone was flown pre-, during and post-development of the bar phases to process any planform changes that might occur. Unfortunately, due to equipment failure, phase 1 final, phase 2 pre-bar, and phase 2 final could not be photographed with the DJI Mavic 2 Pro, so a DJI Mavic Mini drone was used instead. Although DEMs were still acquired, due to the lower resolution and weight which caused shakiness of the DJI Mavic Mini, the post processed DEMs exhibited increased noise compared to the flights flown with the DJI Mavic 2 Pro. It was also found that flights that used two different drone models exhibited increased noise when difference models were created.

A total station and DGPS were used to precisely measure the coordinates of the permanent ground control points (GCPs), which were laid out in a zigzag pattern. Every time the drone was flown, these GCPs were taken and calibrated with Pix4D to guarantee spatial accuracy. The drone georeferencing was validated using a minimum of 6 and a maximum of 12GCPs.

Prior to processing the drone images, a manual review of the photos was performed to remove any photos that were blurry and would affect the final DEM quality. When the upstream water basin was included in the post-processing of the drone footage, there was a significant

amount of noise, especially present when processing the images taken by the DJI Mavic Mini. In order to reduce the amount of noise present, the DEM border was restricted to include only the river and not the upstream or downstream basin. The structure of the OERF, however, made it impossible to entirely remove all the water, and as a result, there was more noise at both ends of the river. Due to the fact that these photos were frequently found at the grid's boundary, this had no effect on the study area. In addition to accuracy, the smaller processing area allowed the DEMs to be processed in a more time efficient manner.

DoD (DEMs of Differences) calculations were performed using ArcGIS to identify any bathymetric changes in the river, including erosion and deposition. The DEMs solely depict changes caused naturally by the river as modifications brought about by human intervention, such as building the bar and digging the pool, were removed from the DEMs. As there is noise present in the DEMs, only changes greater than 2.5 cm were analyzed. To illustrate the changes that occurred in the bed and banks during the different phases, cross-sections were extracted from the DEMs in GIS.

5 ADV results

5.1 Velocity

5.1.1 Near-bank velocity measurements

Near-bank average velocities (within 0.25 m of the right bank) are presented first in Figure 12. Table 1 shows the near bank spatially averaged water velocities. In phase 0, no difference in near-bank velocity was expected between cross-sections. However, the mean velocity at LOWP cross-section was faster than at the two other cross-sections, although not statistically significant ($p>0.05$) (Table 1, Figure 12).

The highest mean velocity (0.91 m/s) was measured in phase 3 at the LOWP cross-section. This was significantly different ($p<0.05$) as it was more than twice as fast as the velocity measured at UPP (0.43 m/s), indicating an acceleration of the flow as it is constricted by the perturbation. There was also a significant difference in phase 3 between cross-section LOWP which had a higher

velocity and DOWN which had a lower velocity ($p<0.05$). For the other phases (smaller or absent perturbations), there were no significant differences in mean velocity ($p>0.05$) between cross-sections with the exception of phase 2 between UPP (lower velocity) and MIDP ($p<0.05$) which was mostly likely due to deeper water caused by the backwater effect. The water surface levels were measured and verified with the total station, confirming the increase in depth.

Phase 1 exhibited only small differences (0.08 m/s) in mean velocity between the MIDP (0.71 m/s) and UPP cross-sections (0.63 m/s) and no statistical difference ($p>0.05$). Spatially, the average velocities were similar between the four cross sections. When compared to phase 0, phase 1 shows an overall increase in velocity although no significance in noted ($p>0.05$).

For a given cross-sections located upstream of the perturbation (UPP), there was a marked significant decrease ($p<0.05$) between phase 2 (0.70 m/s) and phase 3 (0.43 m/s) which may be attributed to the increase in water depth due to the backwater effect. The second largest difference (0.22 m/s) in mean velocities was at LOWP between phase 3 (0.91 m/s) and phase 0 and 1 (0.69 m/s) although not significant ($p>0.05$). Downstream of the perturbation (DOWN), velocity was also unexpectedly reduced between phase 2 (0.70 m/s) and phase 3 (0.52 m/s) but was also not significant ($p>0.05$). Although this was unexpected, drone video of the river shows the flow moving away from the right bank (following the perturbation) and this might have contributed to local velocity decreases.

Table 1: Average velocities of the near bank locations categorized by the four phases and four cross-sections.

Phase	Cross -section	Mean Velocity (m/s)	Min Velocity (m/s)	Max Velocity (m/s)	Standard Deviation (m/s)	N
0	DOWN	0.54	0.41	0.75	0.11	15
0	LOWP	0.69	0.51	0.87	0.12	14
0	UPP	0.57	0.14	0.93	0.22	14
1	DOWN	0.65	0.35	0.85	0.16	22
1	LOWP	0.69	0.32	1.04	0.18	26
1	MIDP	0.71	0.41	1.02	0.17	19
1	UPP	0.63	0.35	0.90	0.18	18
2	DOWN	0.70	0.37	1.00	0.17	25
2	LOWP	0.72	0.08	1.07	0.25	30
2	MIDP	0.56	0.08	1.00	0.26	24
2	UPP	0.70	0.35	0.97	0.16	32
3	DOWN	0.52	0.18	1.00	0.26	22
3	LOWP	0.91	0.49	1.21	0.21	19
3	MIDP	0.63	0.31	0.94	0.20	19
3	UPP	0.43	0.14	0.82	0.18	25

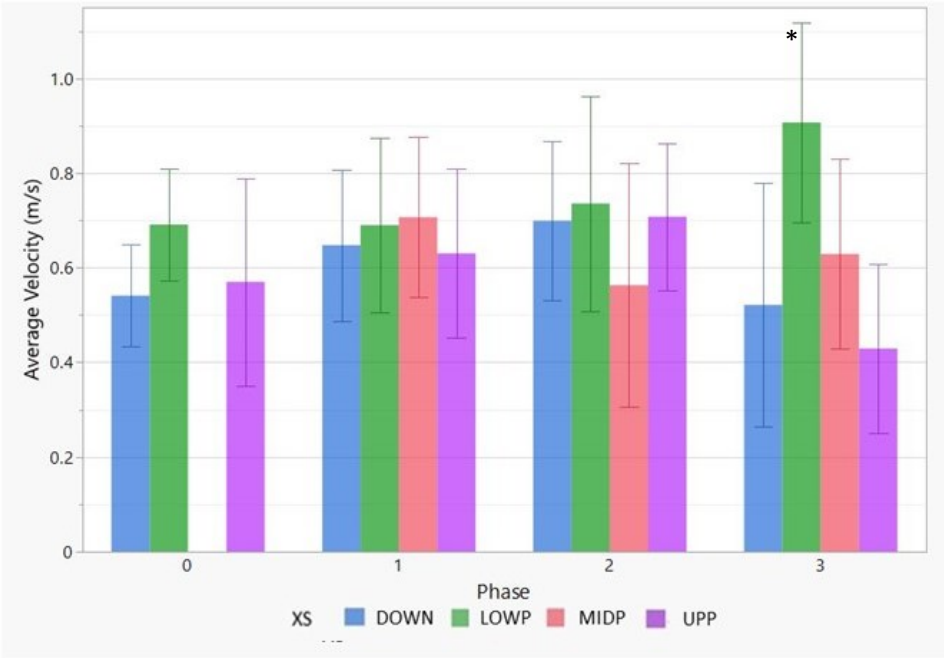

*Figure 12: Average velocity (m/s) of the near bank measurements shown by phase and sub-divided by cross-section. Vertical bars represent standard deviations. An * represents if one cross-section has a signifigant difference from the other cross-sections of a given phase. In phase 3 LOWP had a significant difference from the other cross-sections with the exception of MIDP where there was no statistical difference.*

When viewing individual data measurements, LOWP had the highest mean velocity in phase 3 for every height above the bed (Figure 13). This pattern is repeated in phase 2, but only for the two highest heights above the bed (for 0.10 and 0.15 cm). In phase 3, there is a larger difference in velocity between the points closer to the bank and those further away. This difference between near-bank velocities gradually decreases in phase 2 (for elevations below 0.10 m above the bed) and becomes even less pronounced in phase 1. Phase 0 shows the smallest difference in near-bank velocities.

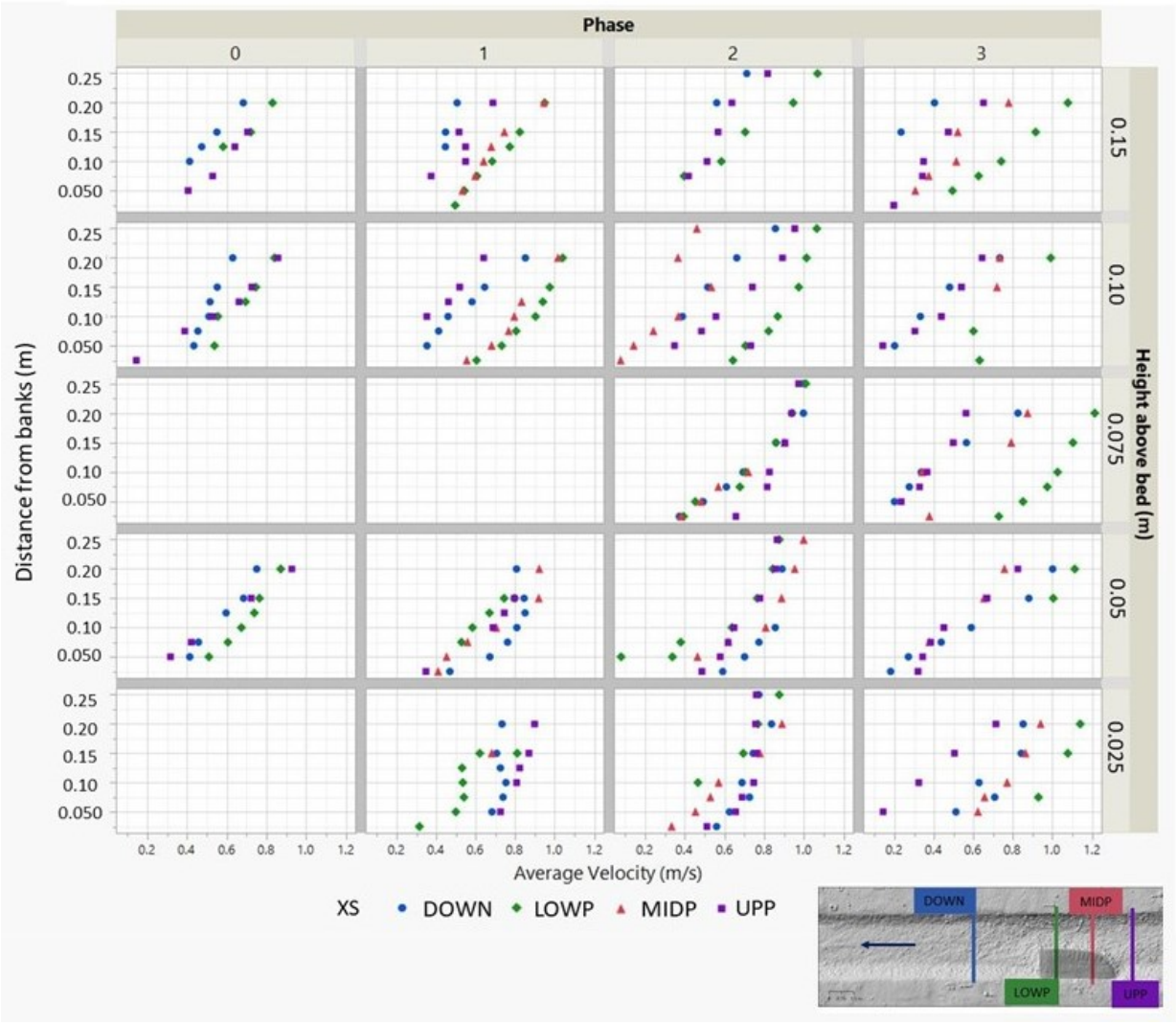

Figure 13: Average velocity for bank velocity measurements at different heights above the bed and different distances from the banks for phase 0, 1, 2 and 3 for the different surveyed cross-sections.

5.1.2 Midstream bed velocity measurements

The spatially average velocities measured in the centre of the channel (at 1.0, 1.4 and 1.8 m from the right bank) are shown in Table 2. The cross-section LOWP, which was where the perturbation was widest, was systematically faster than the other cross-sections, for all phases (Figure 14). For both phase 2 and 3 the cross-section LOWP was significantly faster than the UPP cross-section ($p<0.05$). There is a general trend of increasing velocity from phase 1 to phase 3 for each cross-section although it is not statistically significant ($p>0.05$). The highest mean velocity (1.40 m/s) was in phase 3 at LOWP (Figure 14) whereas the lowest mean velocity (0.95 m/s) was observed in phase 2 at cross-section UPP. The maximum velocity (1.76 m/s) was measured at the LOWP cross-section 37 in phase 3 (Table 2).

The largest difference between cross-section velocities occurred between the slower UPP and faster LOWP (Figure 14). In phase 1, this difference was less (0.24 m/s) but all three phases follow the same trend of a progressive acceleration of the flow from upstream of the perturbation (UPP) to the middle (MIDP) and lower perturbation (LOWP). Finally, in phase 0, where no significant differences between cross-sections are expected, the downstream cross-section (DOWN) was slightly slower from cross-section LOWP ($p>0.05$). The increase in velocity for the midstream positions from phase 1 to 3 was in the range of 0.25 m/s for all cross-sections (Table 2).

Table 2: Average velocities of the midstream near bed locations categorized by the four phases and four cross-sections.

Phase	Cross -section	Mean Velocity (m/s)	Min Velocity (m/s)	Max Velocity (m/s)	Standard Deviation (m/s)	N
0	DOWN	1.04	0.85	1.24	0.14	12
0	LOWP	1.17	0.98	1.41	0.14	12
0	UPP	1.17	1.03	1.32	0.10	7
1	DOWN	1.13	0.87	1.50	0.19	16
1	LOWP	1.20	0.87	1.50	0.19	14
1	MIDP	1.06	0.70	1.33	0.22	13
1	UPP	0.96	0.68	1.25	0.18	13
2	DOWN	1.15	0.66	1.67	0.29	15
2	LOWP	1.31	0.97	1.56	0.17	14
2	MIDP	1.16	0.86	1.44	0.17	16
2	UPP	0.95	0.73	1.18	0.14	15
3	DOWN	1.30	1.05	1.67	0.22	13
3	LOWP	1.40	1.01	1.76	0.23	21
3	MIDP	1.30	0.96	1.58	0.17	21
3	UPP	1.06	0.74	1.42	0.21	18

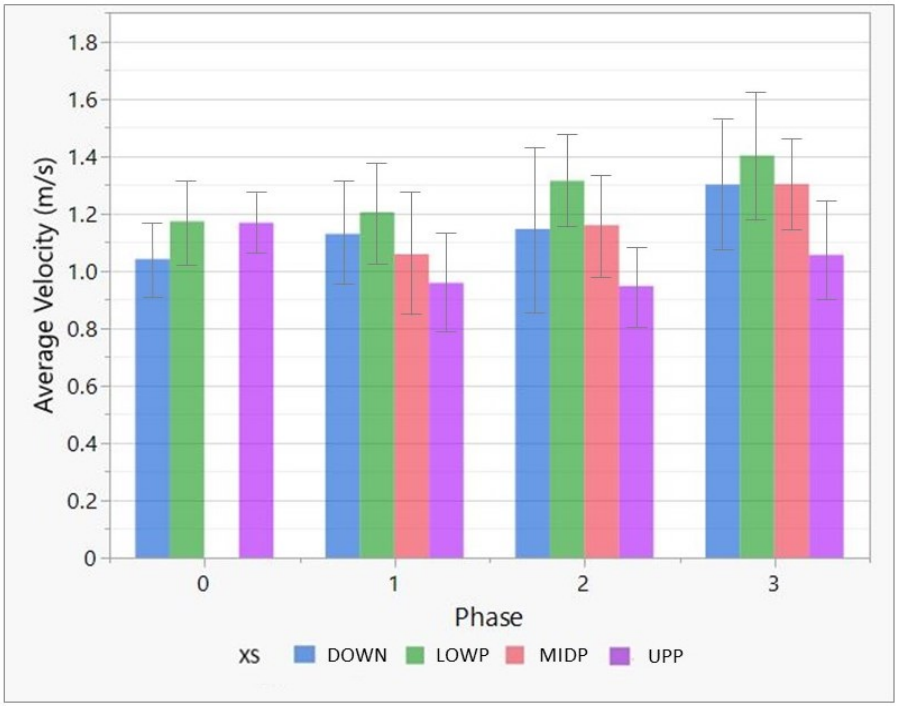

Figure 14: Average velocity (m/s) of the near bed midstream measurements shown by phase and sub-divided by cross-section. Vertical bars represent standard deviations.

More trends can be observed when individual velocity profiles measurements are investigated (Figure 15). As expected, there are no marked differences between the three midstream positions. Most profiles exhibit a logarithmic increase in velocity with height above the bed.

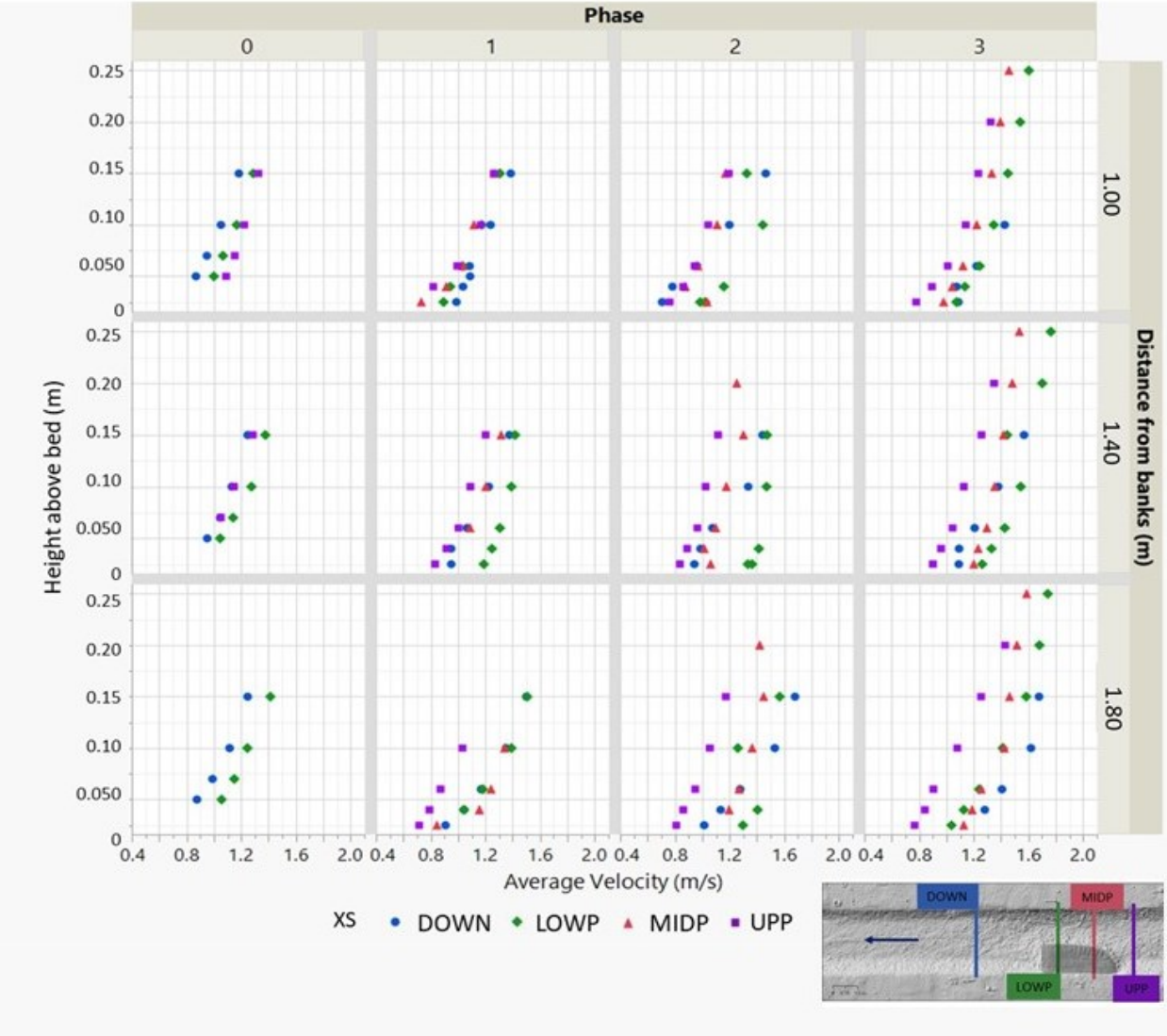

Figure 15: Average velocity for bed velocity measurements at different heights above the bed and different distances from the banks (midstream) for phase 0,1,2 and 3 for the different surveyed cross-sections.

5.1.3 Near-bank velocity vectors

5.1.3.1 Planar velocity vectors

Overall, the presence of a perturbation had only a minor effect on the flow vectors, with the planform angle around 1 to 8 degrees directed towards the right bank at the LOWP cross-section from phase 1 (Figure 16). In phase 2, and even more so in phase 3, the planform angle becomes more pronounced towards the right bank when compared to the previous phase. The vectors of phase 3 are 4 to 12 degrees angled towards the right bank at the LOWP cross-section. The highest flow deflection is noted at the MIDP cross-section for phase 3, with angles of 15-30 degrees towards the right bank, specifically seen at the close to bank points (Figure 16).

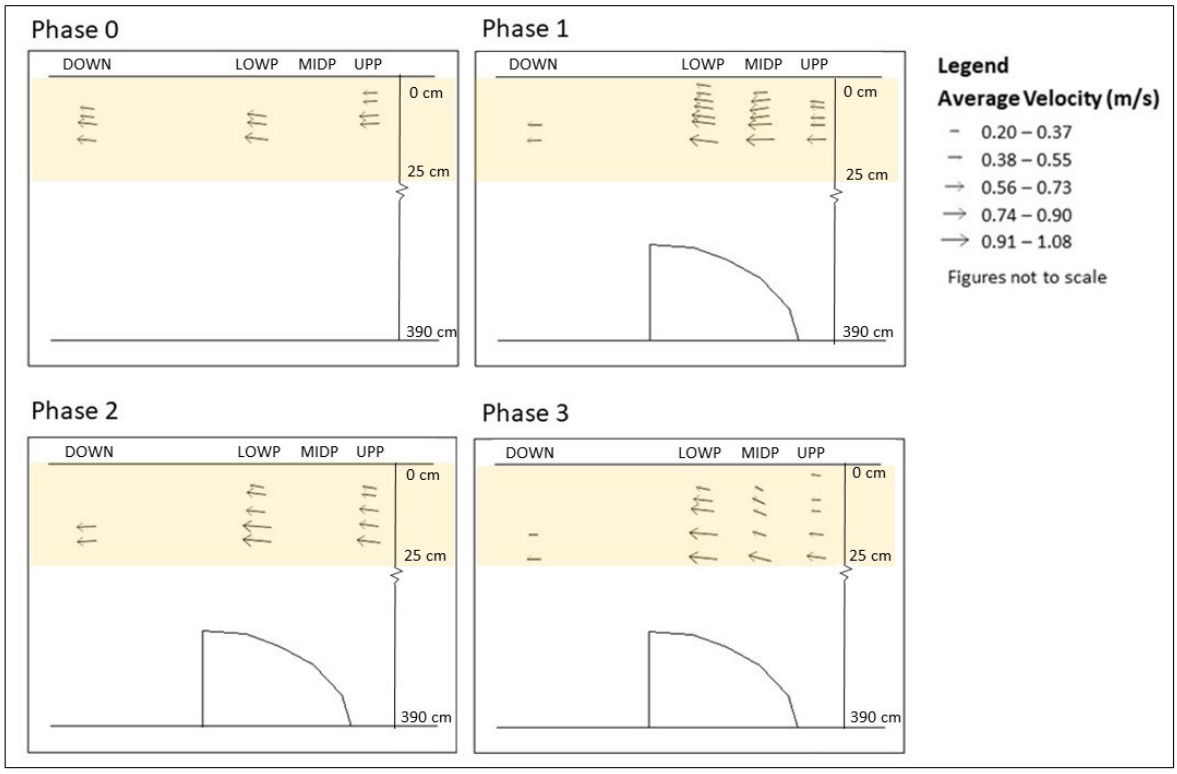

Figure 16: Velocity vectors showing direction and magnitude of the water velocities for the four phases at 15 cm above the bed. The yellow highlighted area (see bottom right-hand map) shows the sampling distance from the right bank.

Drone footage from phase 3 revealed that the surface water flow pattern began to shift towards the right bank. When the water encountered the perturbation, it was diverted from largely straight flow towards the right bank, as was also seen in the results shown by the planform velocity vectors. Following the perturbation, the water is seen directed from the right bank towards to the

left bank, indicating that the addition of the perturbation caused the flow to become slightly sinuous. The supplementary videos "OERF river flow upstream" and "OERF birds eye view" both showcase the water surface patterns.

Videos of the river flow patterns can be found at the following link:
https://drive.google.com/drive/folders/1M8AyFKrNzIEjITS-M-mkGQZKw0BJ8pmZ?usp=sharing

5.1.3.2 Near-bank secondary velocity vectors

The near-bank secondary flow vectors (VW) are presented on top of interpolated maps of the velocity magnitude in Figure 17. The maximum lateral velocity was 0.21 m/s for phase 2, and the average lateral velocity of all phases was 0.071 m/s.

In phase 0, very limited secondary flow is expected since the channel is straight. The mean lateral and vertical velocity for this phase are 0.07 m/s and 0.03 m/s, respectively, indicating that there was nevertheless some cross-stream circulation near the bank. For phase 1, the overall pattern is oriented towards the left bank. However, at the LOWP cross section, flow higher up in the water column is oriented towards the right bank, with near-bed flow towards the left bank, indicating a possible spiral motion. In phases 2 and 3, the orientation of VW vectors is highly variable, but is predominantly oriented towards the right bank for cross-sections UPP, MIDP and LOWP (Figure 17). Overall, the vectors show no evidence of secondary flow currents, which could be due to the fact that the sampled region only encompasses a very small portion of the cross-sectional area, as well as no meander formation occurred.

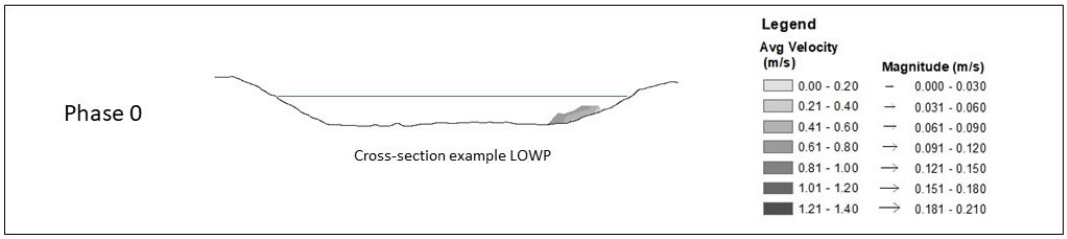
Phase 0
Cross-section example LOWP
Legend
Avg Velocity (m/s)
Magnitude (m/s)
0.00 - 0.20
0.21 - 0.40
0.41 - 0.60
0.61 - 0.80
0.81 - 1.00
1.01 - 1.20
1.21 - 1.40
0.000 - 0.030
0.031 - 0.060
0.061 - 0.090
0.091 - 0.120
0.121 - 0.150
0.151 - 0.180
0.181 - 0.210

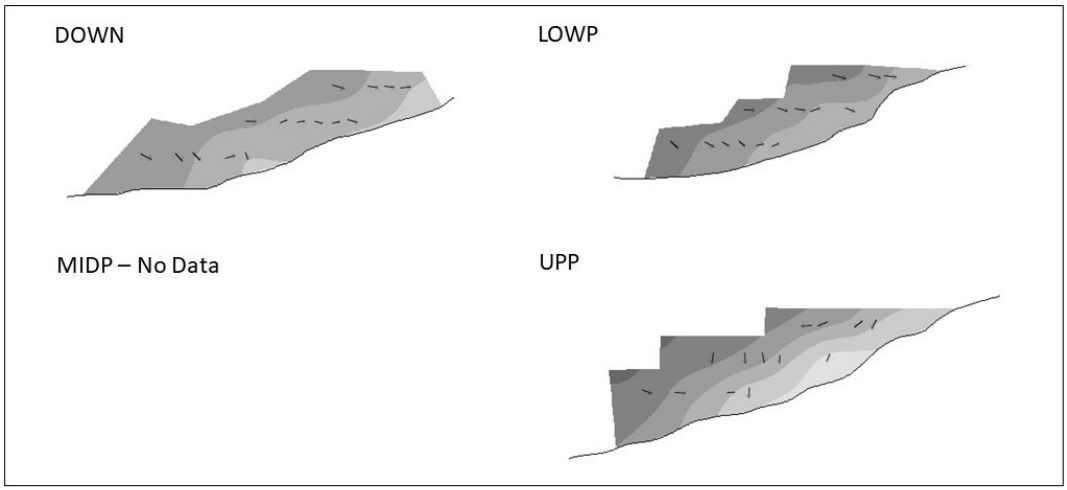
DOWN
LOWP
MIDP – No Data
UPP

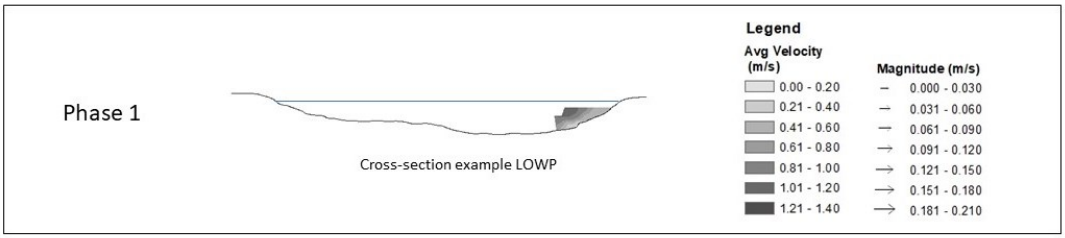
Phase 1
Cross-section example LOWP
Legend
Avg Velocity (m/s)
Magnitude (m/s)
0.00 - 0.20
0.21 - 0.40
0.41 - 0.60
0.61 - 0.80
0.81 - 1.00
1.01 - 1.20
1.21 - 1.40
0.000 - 0.030
0.031 - 0.060
0.061 - 0.090
0.091 - 0.120
0.121 - 0.150
0.151 - 0.180
0.181 - 0.210

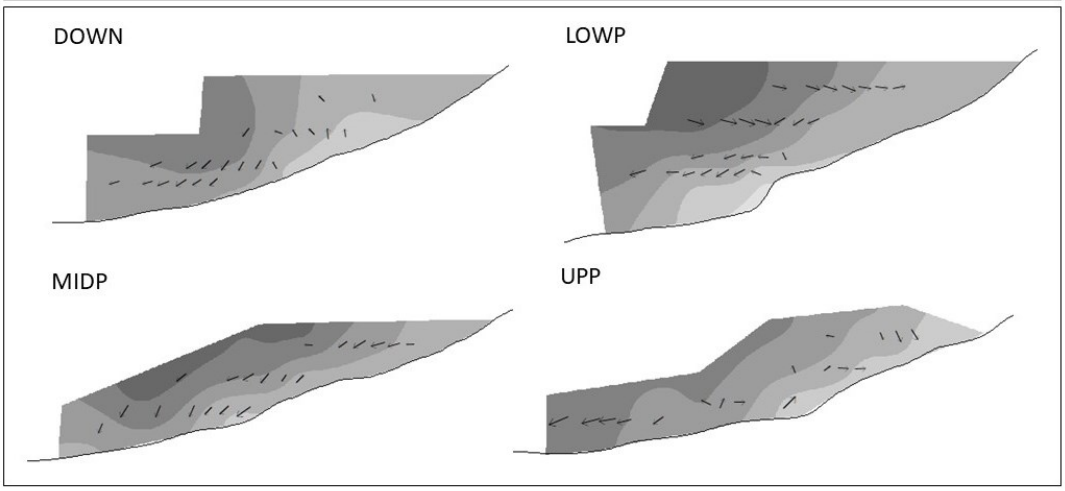
DOWN
LOWP
MIDP
UPP

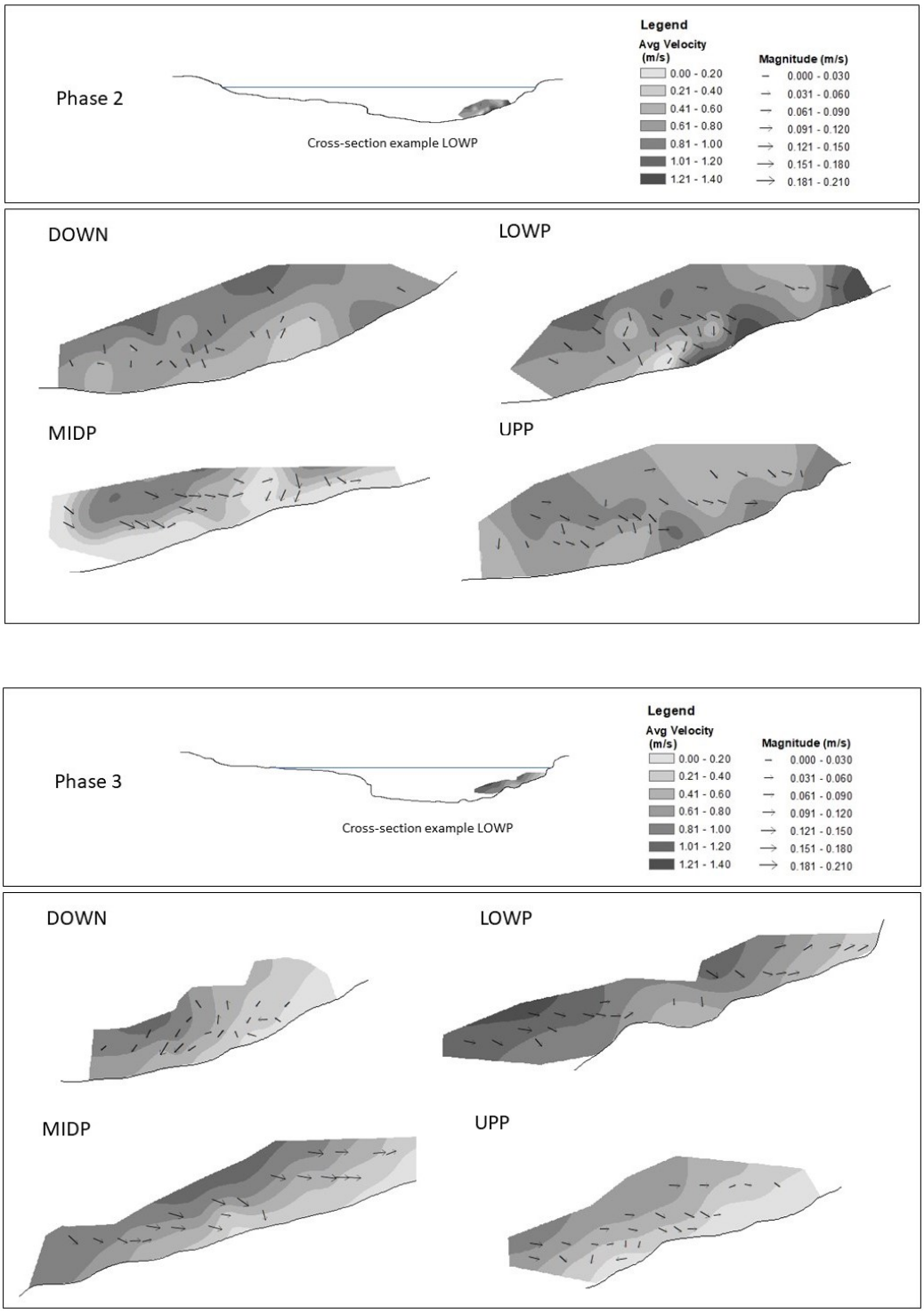

Figure 17: Cross-sectional (VW) vectors superimposed on interpolated velocity magnitude for each phase and each sampled cross-section. An example of the sampled area in each phase is provided for one of the cross-sections at the top.

5.2 Shear stress

5.2.1 Bank shear stress measurements

The bank shear stress measurements are shown in Table 3. Bank shear stress estimated using the log method (horizontal 'perpendicular' near bed measurements) were systematically larger, than for the other methods (Figure 18). However, the log method was only significantly different ($p<0.05$) from the quadratic and Reynolds method but did not show significant differences from the TKE method ($p>0.05$). The TKE method was also significantly different than the quadratic and Reynolds shear stress ($p<0.05$). Between the individual phases and individual cross-sections there were no significant differences ($p>0.05$). Since, as highlighted in Figure 13, velocity increased the most with distance from the bank in phase 3, it is not surprising that the highest log shear stress measurement (28.3 N/m^2) was found for this phase, at cross-section LOWP. The highest log shear stress value was also observed at LOWP cross-section in phase 2 (23.9 N/m^2). With the TKE method, the highest shear stress values were always observed at cross-sections MIDP and LOWP. Larger Reynolds shear stress values were also observed at LOWP and MIDP, but in the range of 6.0 N/m^2 for phase 2 and 3 (thus lower than with the TKE method). There are not marked differences in Reynolds shear stress between phase 0 and phase 1 for these two cross-sections. Similar shear stress values were obtained for all phases using the quadratic method. It should be noted that the logarithmic curve did not follow the logarithmic profile, and so it was difficult to calculate shear stress using the log and Reynolds methods.

Table 3: Shear stress values for the near bank measurements of the four phases and four cross-sections estimated with different methods.

Phase	Cross -section	Log method N/m²	Quadratic N/m²	Reynolds N/m²	TKE N/m²
0	DOWN	12.8	2.1	3.7	5.7
0	LOWP	9.1	3.4	3.9	5.4
0	UPP	20.3	2.6	3.8	7.1
1	DOWN	6.8	3.1	3.0	5.7
1	LOWP	9.7	3.6	3.7	7.0
1	MIDP	10.4	3.7	3.6	9.0
1	UPP	13.1	3.0	2.9	6.9
2	DOWN	16.1	3.6	3.8	6.9
2	LOWP	23.9	4.0	4.9	8.2
2	MIDP	12.1	2.2	6.4	8.6
2	UPP	6.8	3.6	4.3	6.9
3	DOWN	22.2	2.3	3.9	5.7
3	LOWP	28.3	5.2	6.8	8.1
3	MIDP	22.3	2.9	5.6	8.2
3	UPP	14.0	1.5	3.8	5.1

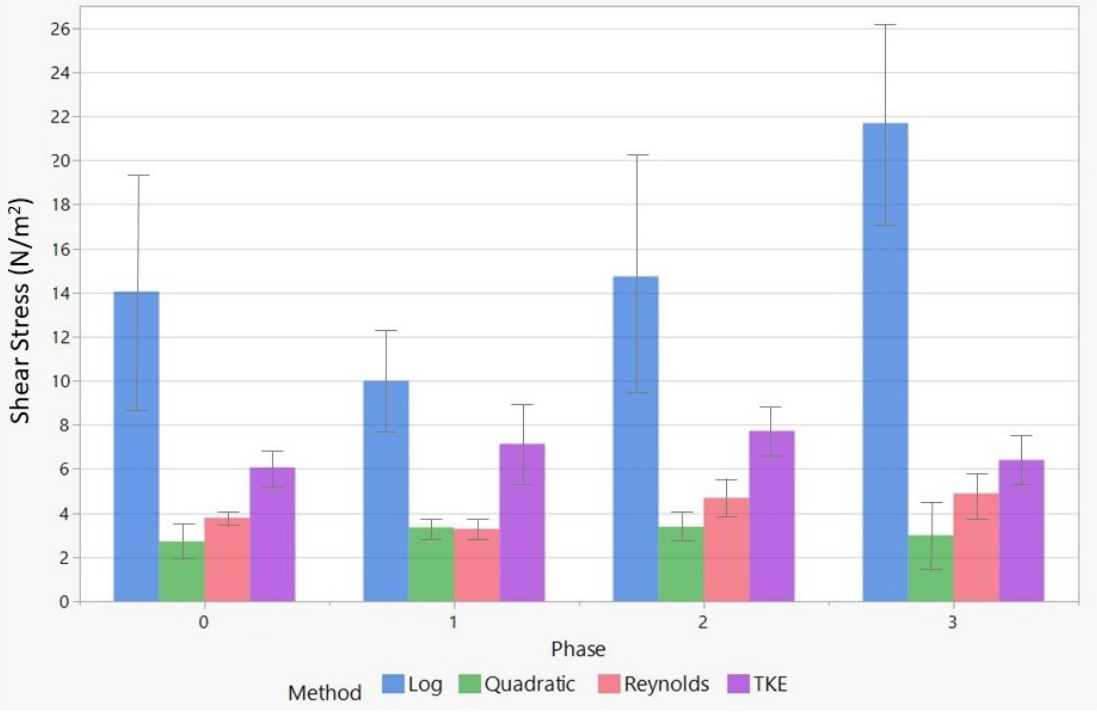

Figure 18: Average shear stress for near bank measurements shown by phase estimated with different methods. Vertical bars represent standard deviations.

There is no obvious way to determine the optimal distance from the bank to estimate bank shear stress using the TKE method. Figure 19 presents individual TKE shear stress estimates for various heights above the bed and from the banks. The shear stress of the UPP cross-section sometimes decreases as the distance from the banks increases, which is expected, but unexpectedly, there are some opposite patterns visible. Overall, it is difficult to identify a clear pattern and determine at what distance from the bank velocity measurements should be taken to obtain reliable bank shear stress estimates.

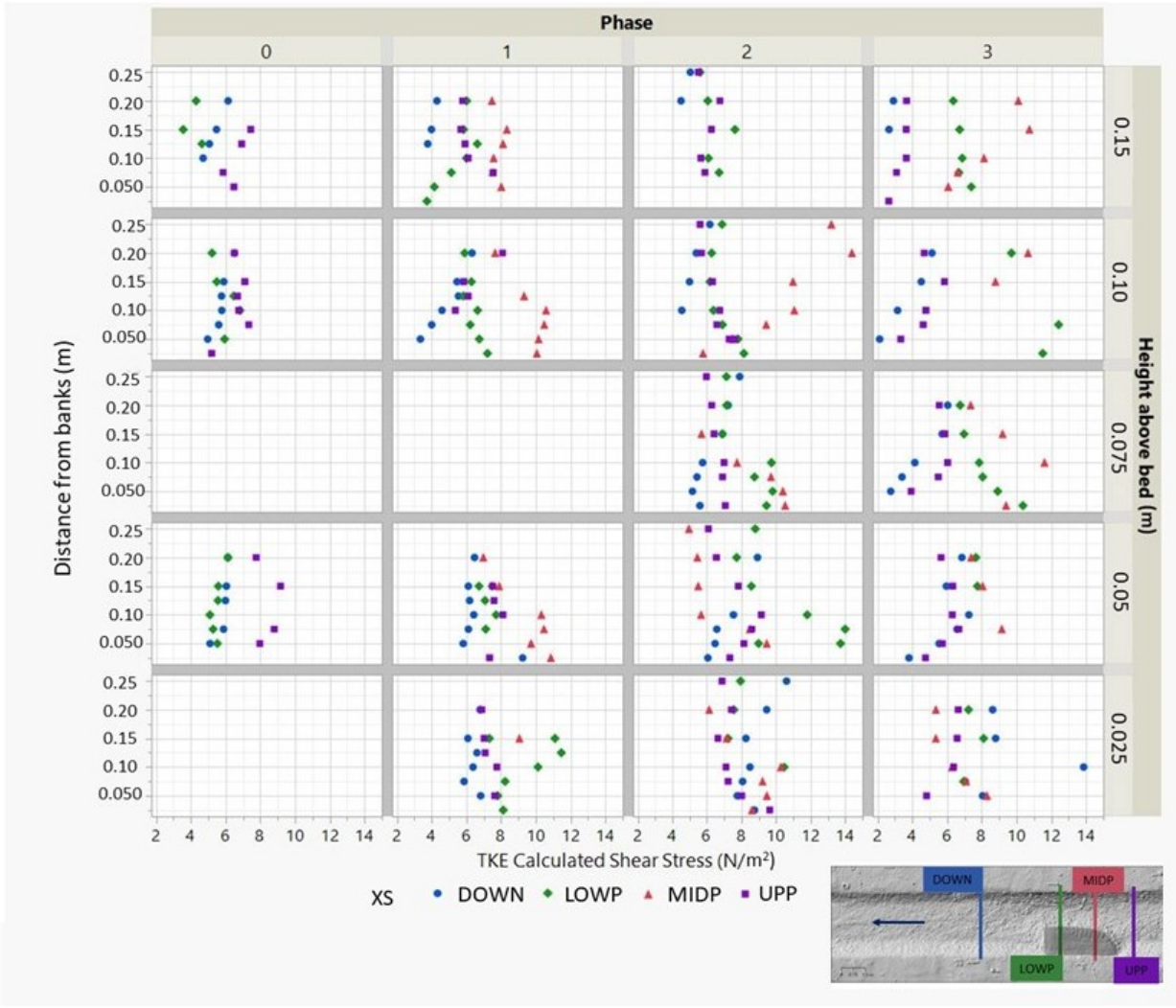

Figure 1919: TKE shear stress for bank velocity measurements at different heights above the bed and different distances from banks for phase 0, 1, 2 and 3 for the different surveyed cross-sections.

5.2.2 Midstream bed shear stress measurements

The midstream bed shear stress measurements are shown in Table 4, with average values per phase presented in Figure 20. There were significant differences between the methods, including between the log method and both the quadratic and Reynolds methods ($p<0.05$), as well as the TKE method and the Reynolds method ($p<0.05$). There were, however, no significant differences between the individual phases and individual cross-sections ($p>0.05$). For the log method, there are small differences between phases and between cross-sections which may be due to the presence of an obstacle. The log bed shear stress for phase 0 is on average 12.5 N/m^2, which is very similar to the slope-depth average bed shear stress of 12.3 N/m^2 (equation 1). The other methods which give markedly lower values of bed shear stress for phase 0 (an average of 6.9 N/m^2 for TKE and only 0.9 N/m^2 for Reynolds), may indicate some limitations in the ADV turbulence measurements. The highest shear stress was measured in phase 1 at cross-section UPP (23.4 N/m^2). With TKE, the highest mean shear stress (10.1 N/m2) was in phase 2 at the DOWN cross-section. For Reynold's shear stress the highest shear stress (5.0 N/m^2) was in phase 3 at the LOWP cross-section.

Table 4: Shear stress estimates for the midstream near bed measurements of the four phases and four cross-sections estimated with different methods.

Phase	Cross -section	Log N/m^2	Quadratic N/m^2	Reynolds N/m^2	TKE N/m^2
0	DOWN	14.9	3.8	1.6	6.7
0	LOWP	10.1	4.2	2.3	7.1
0	UPP	12.5	4.1	1.0	7.0
1	DOWN	10.8	4.4	4.4	9.1
1	LOWP	17.3	4.8	2.9	5.7
1	MIDP	13.6	4.2	2.3	9.2
1	UPP	23.4	3.8	3.6	6.5
2	DOWN	2.5	4.7	2.0	10.1
2	LOWP	15.3	4.8	1.8	4.1
2	MIDP	6.2	4.2	3.5	5.8
2	UPP	14.3	3.6	3.2	7.2
3	DOWN	11.1	5.1	3.1	9.9
3	LOWP	6.2	5.0	5.0	6.7
3	MIDP	22.3	4.6	1.9	5.9
3	UPP	14.0	4.3	4.2	6.7

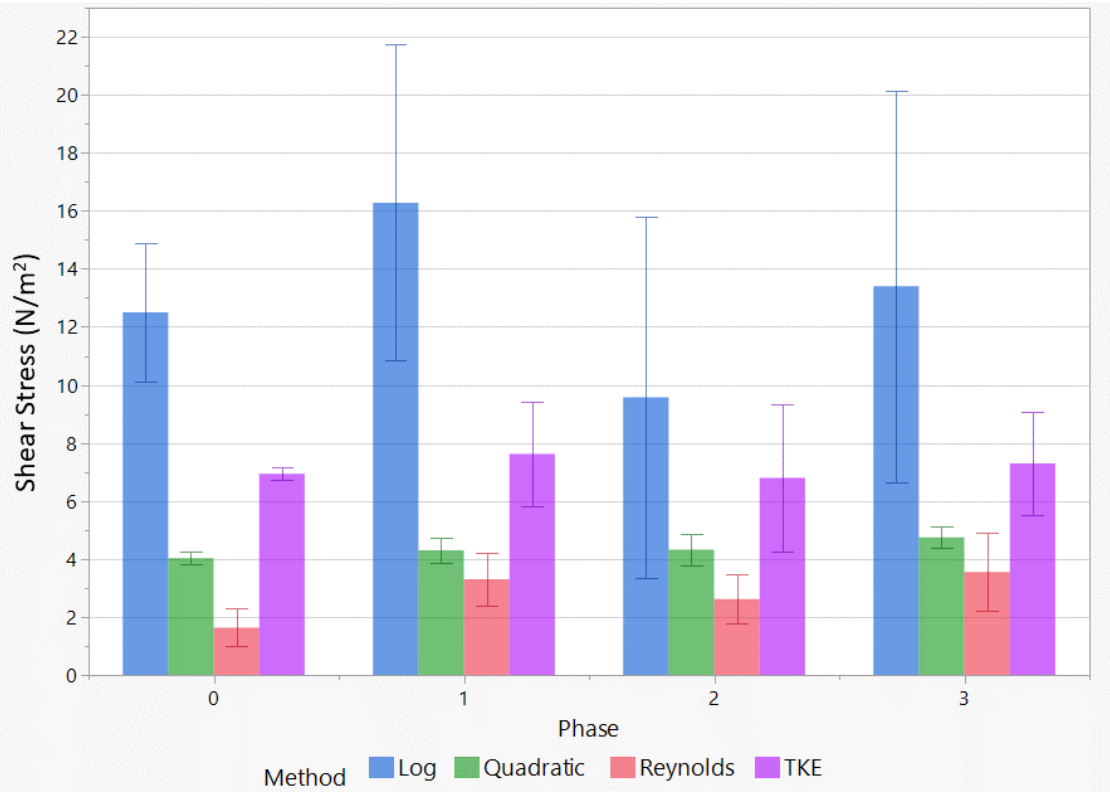

Figure 20: Shear stress for near bed measurements shown by phase and sub-divided by cross- section estimated with different methods. Vertical bars represent standard deviations.

6 Drones and visual observation results

The DEMs created from drone imagery with SfM reveal that relatively minor changes have occurred with each phase (Figure 21). As expected, phase 3 was more dynamic than the previous phases, with signs of erosion and deposition (Figures 21c). The upper part of the bank exhibits a vertical edge (top 0.05 m) that was eroded (Figure 22a and b). Downstream of the perturbation, these vertical edges continued for another 2 m before gradually decreasing (Figure 22a and b).

Erosional lines were observed on the left bank upstream of the disturbance, where there was a clear thin line of erosion at the waterline (3-5 m upstream of the MIDP cross-section) (Figure 22c). On the left bank downstream of the perturbation, there was a buildup of fine sediments starting in phase 2 (Figure 21c and 22d). This area corresponds to much slower velocity and recirculation flow, as noted in drone video footages. Although not as marked as upstream, the water began to cut into the left bank again midstream (22.5 m) (Figure 22e).

In phase 1, erosion was minor across the perturbation on the right bank, ranging from 0.025 to 0.05 m (Figure 21a). Throughout the river there was a minor amount of deposition (2.5 to 5.0 cm). In the center of the river downstream from the perturbation, deposition ranging between 0.025 and 0.075 m was noted in an area of roughly 3 m^2 (Figure 21a). Further downstream, where sediment traps once stood (22.5 m), approximately 0.025 to 0.05 m of deposition occurred over an area of 0.5 m^2.

In phase 2, between 0.025 and 0.075 m of erosion occurred on the right bank across from the perturbation. A small area (0.94 m^2) with erosion ranging between 0.05 and 0.075 m took place on the right bank; it began at the end of the perturbation and lasted for the following 2 m (37 to 35 metre mark). The erosion on the right bank continued downstream of the perturbation, (from the 34 to 22 metre mark), although to a lesser degree. Between 35 and 31 m, a small amount of erosion (0.025 to 0.05 m; around 1.2 m^2) occurred in the centre of the river (Figure 21b).

For phase 3, on the right bank across from the perturbation, erosion ranged between 0.025 and 0.05 m (Figure 21c). The erosion continued diagonally across the river channel, covering an area of approximately 0.68 m^2. Adjacent to the perturbation, there was a midstream deposit of an area of 0.76 m^2 with an elevation change of 0.025 to 0.075 m. Directly beside the perturbation was a noticeably scour area, with the greatest scour occurring at the lower end of the perturbation. Further downstream, along the left bank between 31 and 22.5 m there was a narrow line of erosion (0.025 to 0.075 m). Where the sediment trap was initially situated (22.5 metre mark), there was a limited amount of deposition (0.025 to 0.075 m; 0.35 m^2).

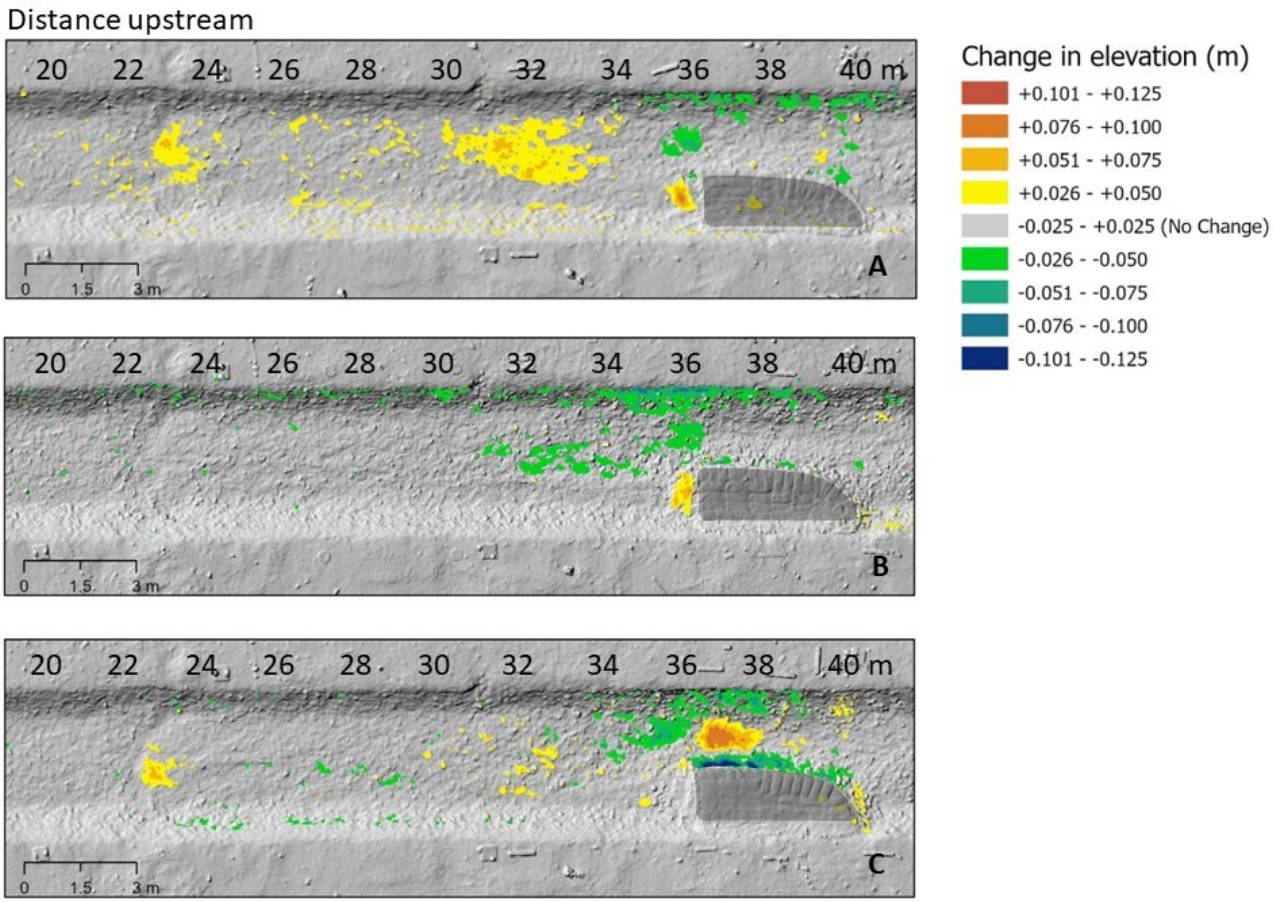

Figure 21: DEM showing the differences in elevation difference before and after for the three phases with perturbation A) difference between phase 1 and phase 0; B) difference between phase 2 and phase 1; C) difference between phase 3 and phase 2. Modifications brought about by human intervention, such as building the bar and digging the pool, were removed from the DEMs.

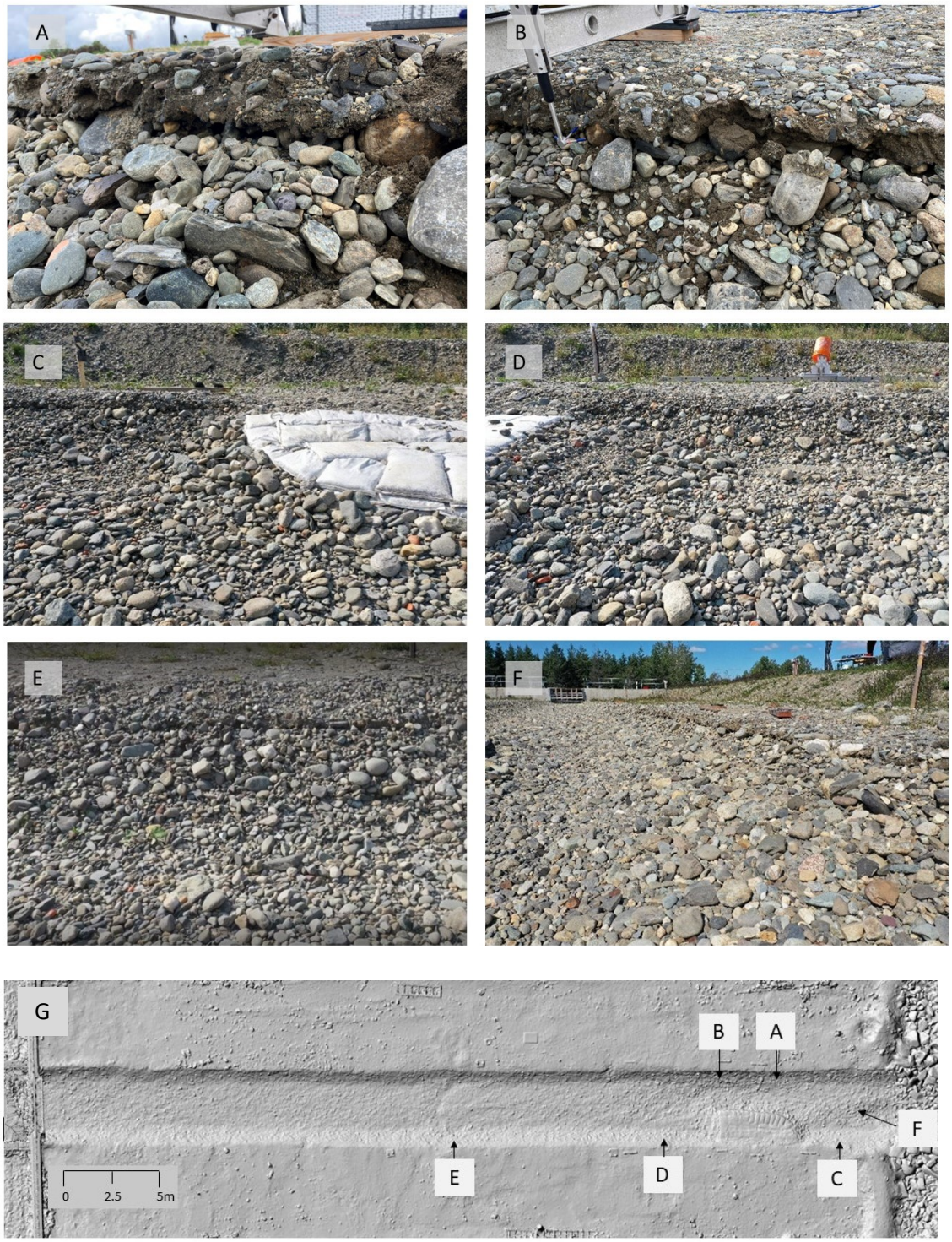

Figure 22: Photograph of the drained river after phase 3. A) upper right bank opposite the perturbation showing visible erosion, B) lower right bank opposite the perturbation showing visible erosion, C) the left riverbank just above the perturbation, and D) the left riverbank just below the perturbation, while E) the midstream left bank (22.5 m), and f) the entire right bank shown from upstream. G) Map represents locations photographs were taken.

6.1 Cross-sectional analysis

Cross-sections extracted from the DEMs (phases 0 to 3) reveal that although there was erosion and deposition, it was minimal in areas without the perturbation (Figure 23). Limited erosion is observed for cross sections, UPP, which is above the perturbation, and DOWN, which is further downstream of the perturbation (Figure 23a and d). The cross-sections at the perturbation, MIDP and LOWP, exhibit more erosion on the right bank (Figure 23b, c, e, and f). The right banks show a continuous amount of erosion occurring between the four phases. This is unlike UPP and DOWN, which only show a small amount of erosion between phases.

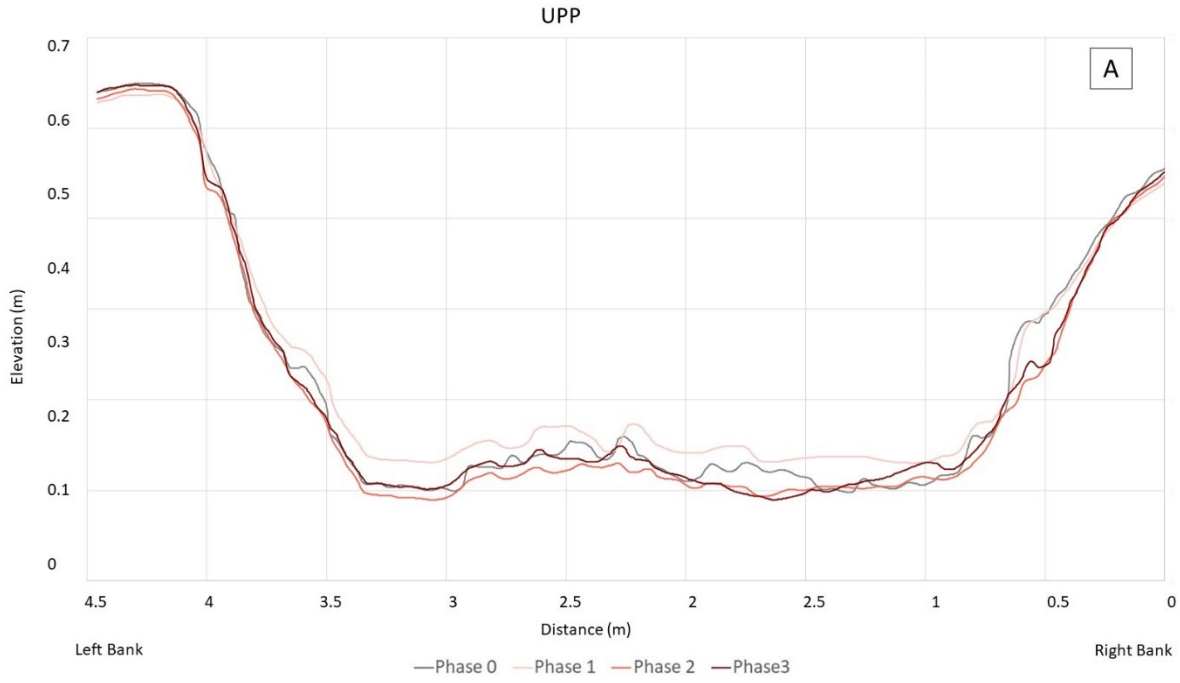

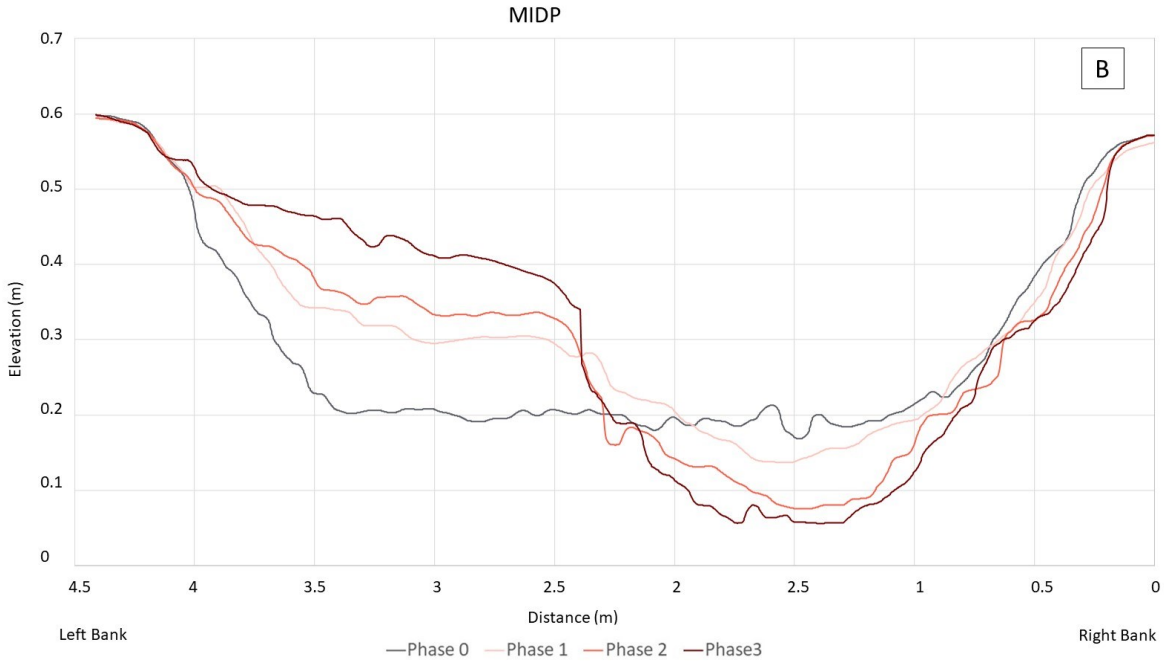
MIDP
B
0.7
0.6
0.5
0.4
0.3
0.2
0.1
0
Elevation (m)
4.5
4
3.5
3
2.5
2
2.5
1
0.5
0
Distance (m)
Left Bank
Right Bank
Phase 0
Phase 1
Phase 2
Phase3

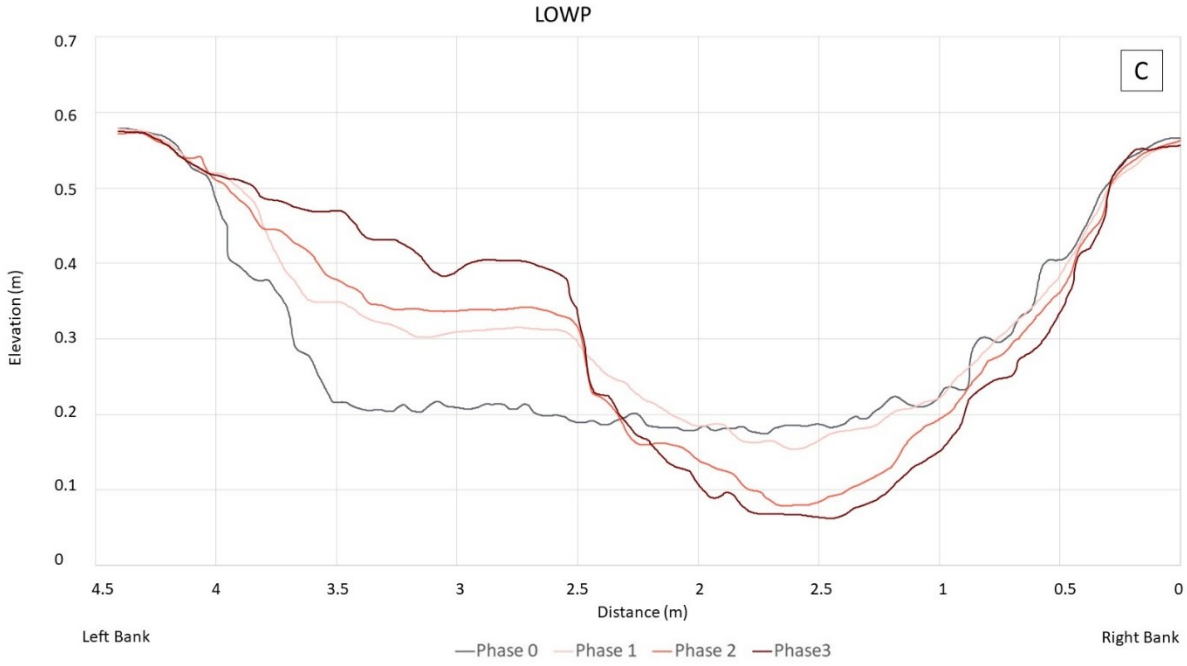
LOWP
C
0.7
0.6
0.5
0.4
0.3
0.2
0.1
0
Elevation (m)
4.5
4
3.5
3
2.5
2
2.5
1
0.5
0
Distance (m)
Left Bank
Right Bank
Phase 0
Phase 1
Phase 2
Phase3

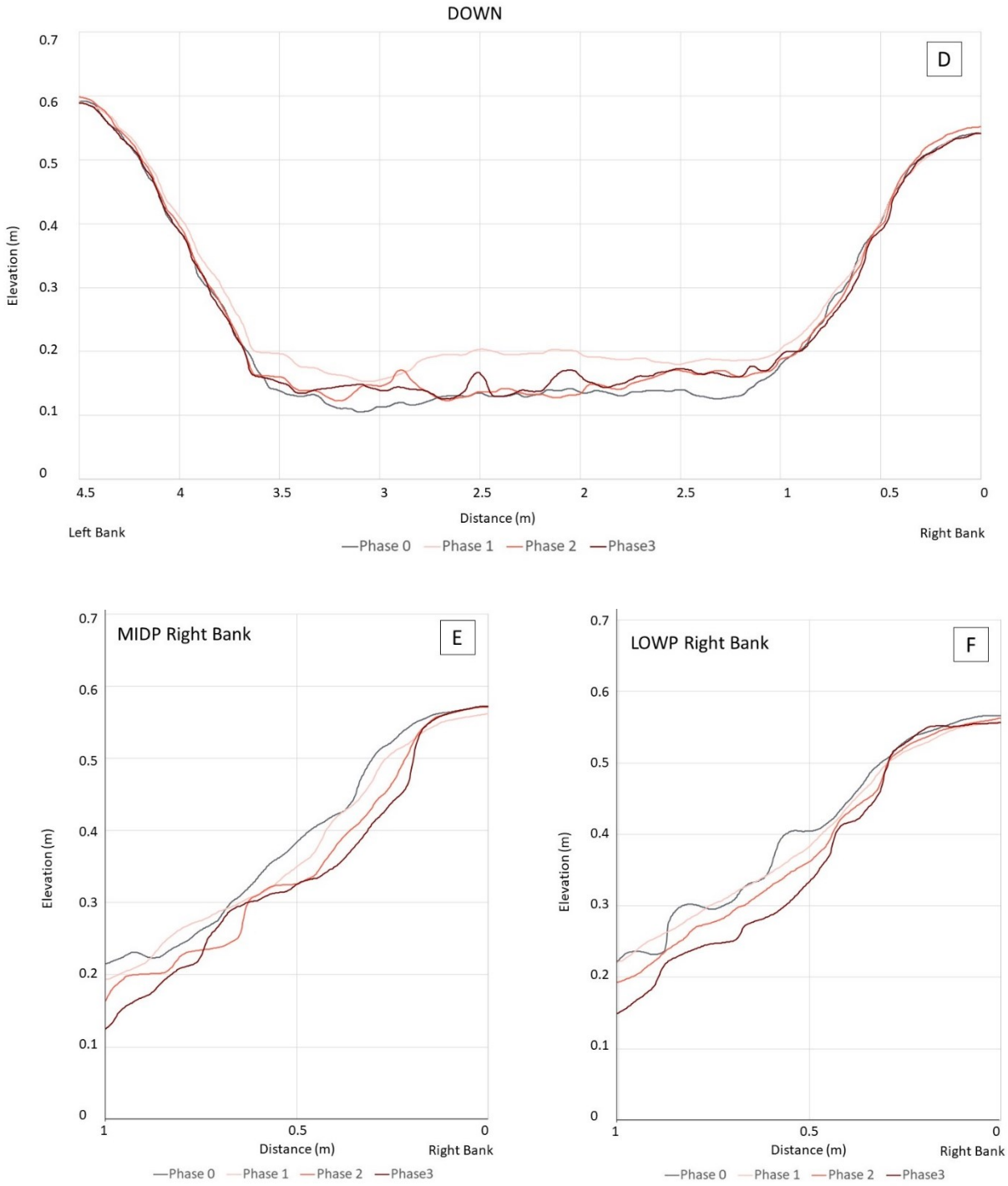

Figure 23: Cross-sections taken from the DEMs A) UPP B) MIDP C) LOWP D) DOWN E) Zoomed in on MIDP right bank and F) Zoomed in on LOWP right bank.

7 Discussion

7.1 Quantifying flow dynamics

There was no meander formation and limited planform evolution changes at the OERF following the addition of an upstream disturbance. There was, however, changes in erosion and deposition patterns as the perturbation sizes increased. The most complex changes to the river were observed in phase 3 (largest perturbation). Phases 1 and 2 saw rapid armouring of the river, where initial erosion and deposition were detected but stopped as the river became armoured. Phase 3 did not armour right away and experienced erosion and deposition for a longer period of time than phase 1 and 2. Phase 3 eventually grew more armoured (although it did not completely armour in the course of the experiments) and therefore only a small amount of erosion continued, albeit at a considerably slower rate as the river become increasingly armoured. Key findings about the geomorphological developments that took place at the experimental river will be discussed below.

7.1.1 Velocity and bank shear stress

In meandering rivers, the highest velocities are observed closer to the inner bend (at the beginning of the meander) with a gradual shift towards the outer bend as the meander progresses downstream (Blanckaert et al., 2012; Pradham et al., 2018,). In a straight river such as at the OERF, the highest velocities are observed in the centre of the channel (Pradham et al., 2018). These expected velocities were similar to the results observed at the OERF with the highest velocity occurring in the centre of the channel. Pradham et al. (2018) found that the narrower cross-sectional area of meanders increases the velocity and drives more water through a smaller area. The results seen at the OERF generally support this, which was specifically evident in phase 3, at the lower perturbation where there was an increase in local velocity compared to the other phases.

From velocity, shear stress is also a key parameter to understand planform evolution. The expectation in this study was that shear stress near the right bank would increase following the addition of the upstream perturbation and would exhibit more spatial variability than for the phase 0 (straight) channel. Indeed, shear stress has been shown to vary depending on the location in a meandering stream (Lin et al., 2021). Higher bank shear stresses are generally found near the outer

curve of a river meander (Stoesser et al., 2010). However, even though the OERF experienced erosion and deposition and some planform evolution, it is still classified as a straight river channel as no sinuosity developed and therefore, the theoretical expected meander shear stress values were not observed.

Eventually, it would be anticipated that if a meander formed at the OERF, the area just downstream of the apex of the bend would experience the largest shear stress on the banks (Stoesser et al., 2010). If the OERF had shown meandering, this would be expected to occur somewhere between the 36 and 39 m mark, just at the end of the perturbation. However, it is challenging to draw any firm conclusions about shear stress readings since the patterns between the four shear stress measuring techniques vary. There is relatively little difference in the shear stress across phases, with the exception of log shear stress which is the only approach that results in estimates substantially larger than the critical shear stress of 7.1 N/m^2 (based on D_{50}=10mm from the initial river). Since very little bank erosion was noted in the DEM analysis, it would appear as though the log method overestimates bank shear stress. TKE measurements are closer to the critical shear stress measurement with only a few values reaching or coming close to 7.1 N/m^2. Initially, there was movement on the bed and banks as shear stress values were close to the critical shear stress. However, as the river armoured, the D_{50} increased from 10 to 23 mm, and thus critical shear stress increased to a value of 16.4 N/m^2. Consequently, the movement on the bed decreased as the river became more armoured.

Previous studies have found similar difficulty in appropriately measuring and quantifying bank shear stress. The impact of spatial and temporal distribution on near bank shear stress and the subsequent bank erosion is poorly understood (Kozarek et al., 2023). In fact, research on calculating bed shear stress is far more advanced than current research on bank shear stress. Using the logarithmic profile with time-averaged velocities to determine bank shear stress near banks, for example, has proven tricky since sloped banks do not follow a logarithmic curve (Hopkinson and Wynn-Thompson, 2016; Kozarek et al., 2023). These findings are comparable to those obtained at the OERF, where the flow field along the banks did not follow a logarithmic profile. Kozarek et al. (2023), when comparing different shear stress estimates on sloped banks at the Outdoor StreamLab (St Anthony Falls Laboratory, University of Minnesota), found no consistent relationship between near bank shear stress calculations and individual turbulent flow statistics. In

addition, there was significant variation between shear stress estimates, a conclusion that was also observed at the OERF. Due to the three-dimensional flow structure generated by the sloped banks, they observed great variability when utilizing turbulent characteristics to predict near bank shear stress in both meandering and straight sections of their experimental channel (Kozarek et al., 2023). Combined with our findings at the OERF, it is clear that quantifying bank shear stress still requires additional research.

7.1.2 Artificial perturbations and meandering rivers

Lewin (1976) investigated an artificially straightened gravel-bed channel with a trapezoidal cross-sectional shape and found that the river channel was only active during high-flow events which enhanced bank erosion. The meander platforms that were created at regularly spaced intervals were mainly a result of secondary flow motions. Following the formation of a sinuous channel, flow patterns became less dependent on the original meander formations, and lateral accretion was observed as a result rather than a precursor to the erosion (Lewin, 1976). This is in contrast to the OERF that did not experience high-flow events as the river maintained a constant flow.

Planform meandering is closely tied to the development of bars and pools, which can be understood as a resonance phenomenon. Blondeaux and Seminara (1985) performed a linear stability analysis of flow in straight erodible channels and found that the wavelength of the instability that leads to alternate bar formation is similar in size to the wavelength at which bends tend to amplify. Their analysis showed that at resonant conditions, curvature of flow in sinuous channels reinforces perturbations of the alternate bar type. They concluded that if bend amplification is allowed to develop, the transient process that begins with an initially straight configuration perturbed by the existence of alternate bars will eventually reach steady state (Blondeaux and Seminara, 1985).

Few studies have looked at the flow dynamic effects of adding a perturbation to a straight river channel. Numerical and physical modelling have shown that the development of chute cutoffs eventually has a substantial impact on the formation of meanders (Braudrick et al., 2009; van Dijk et al., 2013; Weisscher et al., 2019). According to Weisscher et al. (2019), only the first bend of meander development was impacted by the initial inflow perturbation. This might be because the perturbations become dampened as they moved downstream (Zolezzi and Seminara, 2001).

The numerical model of Schuurman et al. (2016) showed that bends and alternate bars were necessary for the downstream propagation of a perturbation in order for sustained meander formation. They also found that grain size, channel curvature perturbation, and width-to-depth ratio were crucial to create high sinuosity meandering. Their numerical model supports the view that maximum velocities occur at channel inflection points rather than at bend apexes (Schuurman et al., 2016). These previous numerical and physical models illustrate, along with the OERF findings, that meander creation is still a challenging issue to study, particularly at larger scales.

7.1.3 ADV sampling limitations

Although ADVs are intended to study turbulent flow, if there is too much turbulence, problems of low correlation can occur. While this does not necessarily result in bad data, it can increase the noise and quality of the ADV data (Doroudian et al., 2010; Martin et al., 2012; Wahl et al., 2012). Random spikes and Doppler noise affect the precision of the ADV and the accuracy of the measured data (Doroudian et al., 2010). Measurements close to the bed are especially challenging to quantify as there is often large spatial average differences due to the non uniformity (Doroudian et al., 2010).

Several ADV points needed to be removed from the analysis in this study. One possible explanation of the decreased quality in the measured ADV data of the OERF was the high roughness on the bed, which led to increased turbulence (Engel and Rhoads, 2017). Although there have been successful cases of ADV used in higher roughness environments (Biron et al., 1998), the OERF locations where measurements were taken may have impacted the quality of results. In phase 0, when the ADV ladder positions were selected, an effort was made to position the ladder where upstream disturbances, such as jutting rocks, would have the least impact. As the sediments of the OERF are naturally sorted there is a considerable variation across the riverbed, as is typical of a gravel-bedded river. The bed topography therefore varied along the cross-sections, and some ADV measurements were measured in less desirable locations, due to interactions with protruding rocks. Although this reduced bias, the result quality may have been nevertheless affected. Additionally, as the river evolved, erosion on the right bank led to even more protruding rocks which can impact mean and turbulent flow fields. Studies have shown that boulders and their resultant vortices can affect momentum exchange (Buffin-Bélanger and Roy, 1998), and erosional and depositional patterns (Liu et al., 2017a) which can impact ADV results.

In addition to the above point, large individual rocks have the ability to degrade the quality of the ADV signal which may be reflected back, adding noise to the measured velocities (Engel and Rhoads, 2012; Martin et al., 2012). At the OERF, some large, isolated rocks could be seen protruding from the banks, and as the banks eroded additional large rocks were further exposed. In areas closer to the banks, this can cause backscattering which can increase the noise and cause data spikes, subsequently decreasing the quality of ADV data measured. This was clear when the ADV was measured physically and found to be a particular distance from the banks, but the computer reading revealed the distance to be continually changing, indicating the presence of phase shifting (Doroudian et al., 2010). This backscattering effect may indicate why many of the data points close to the bank had to be removed in post processing.

Finally, as the ADV has a sampling volume of 1 cm^3, protruding rocks may have contributed negatively to the precision of the data. The OERF has a large flow area compared to flumes, and therefore the ADV values only show a small proportion of the area. In addition, the OERF's bed and banks exhibit a wide range of sediment size and variability. Consequently, many more data points would be needed to adequately reflect the complexity of the flow field. Due to the length of time required to sample ADV data and the size of the OERF, increasing the number of data points sampled was not feasible in this study. It should be noted that the OERF is much less complex to sample than a natural river, and even under these "ideal" sampling conditions it remained challenging to use ADV measurements to determine bank shear stress, as was also noted by Kozarek et al. (2023). Natural rivers are much larger in size than the OERF and will exhibit even more wide ranges of sediment size and variability as well as bank vegetation and irregular bank topography, making it even harder to quantify bank shear stress from point velocity measurements.

7.1.4 Algae complications

Algae present in the system may have had a major impact on measurements of velocity and therefore on the estimation of both bed and bank shear stress. Although every effort was made to mitigate their negative impacts, there was still often algae present on the sampling equipment and therefore the ADV results may have been impacted. Filamentous algae are very fine and stringy, and can easily attach themselves to equipment and rocks. If a larger piece of algae attached itself to the ADV during measurements, a spike could be observed in real time, and as a result the ADV

was cleaned, and a fresh measurement was recorded. Small pieces of algae, however, were difficult to see and might have adhered themselves to the instrument in the middle of a reading, leading to possible data inaccuracies. In order to reduce the impact of algae for future experiments, it is advised that mitigation techniques be attempted before collecting additional ADV measurements.

7.2 Planform evolution and meander formation

The river's visual appearance indicates that during each of the experiments four stages, there was sediment transport, erosion and deposition. Phases 1 and 2 achieved an armoured state more quickly (within one day) than phase 3, which had not yet reached a complete armoured state by the end of the experiments. Once the initial erosion and deposition had taken place during phases 1 and 2, the river appeared visually stable. This was most likely caused by the small size of the pool and bar in phases 1 and 2. That is, during phases 1 and 2, there was sufficient instability to cause initial local adjustments, but the river quickly stabilized, and no further changes occurred. Erosion and deposition were also rapidly observed at the beginning of phase 3. However, unlike phase 1 and 2, the changes persisted even after the river had been run for days, albeit at a slower rate. As a result, it can be concluded that in phase 3, the size of the perturbation decreased the stability of the channel bank, resulting in erosion on the opposite side of the disturbance.

The river started to show very slight sinuous flow as a result of the increasing perturbation sizes. This is suggested by the minor signs of erosion observed on the left bank several metres downstream the perturbation, as well as the videos showing sinuous flow, and the velocity vectors which became more angled towards the right bank as the phases progressed. Even though the OERF is still classified as a straight river channel, this increased erosion (and sinuosity) from the perturbation could start to be seen.

Although there were geomorphological changes that occurred during the experiments, meander formation and large geomorphological changes did not occur. Several factors may explain the lack of meander formation in this study, including 1) the grain size distribution had fractions to large to be mobilized (Turowski et al., 2015) with the maximum flow rate allowed by the OERF pumps; 2) the amount of bank erosion that occurred was limited by cohesive material, sediment composition, and rock placement (Thorne and Tovey, 1981); 3) the experiment was not run for a sufficient amount of time (Braudrick et al., 2009; Kleinham et al., 2009; Salas and Rhoads, 2022);

and finally 4) armouring of the bed without the addition of sediments left the river 'starved' of a sediment supply, which limited erosion and deposition and, consequently, the planform evolution (Braudrick et al., 2009).

At the end of the experiments, many large-sized sediments did not move, indicating that the flow was insufficient to move the entire distribution of sediments. Thus, bank and bed shear stress did not surpass the critical shear stress required for sediment transport (van Rijn, 1984). This meant that there was limited erosion and deposition at the OERF due to the smaller amount of transportation that could take place.

Critical shear stress could have been influenced by high friction angles, cohesion, and instream vegetation. Larger rocks were partially held in place by the banks, as well as by the rocks underneath, which prevented erosion. Very small plants (2 cm) with roots up to 7 cm long were found on the banks, particularly on the left bank (Figure 24). Roots of plants are known to increase cohesion between soil particles, and thus shear strength, restricting the movement of larger particles (Li et al., 2006, Florsheim et al., 2008; Rey, 2009). However, the degree to which the plants limited bank erosion at the OERF remains unknown.

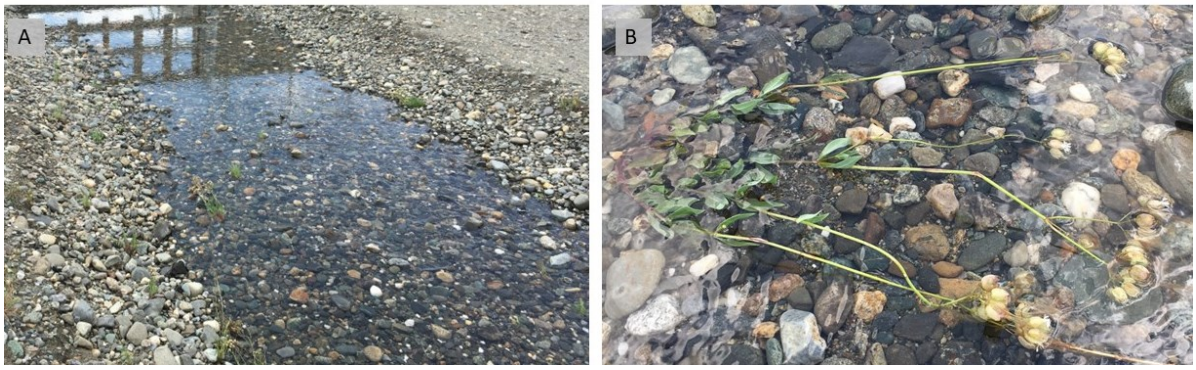

Figure 24: A) Rooted plants in the drained river. Plants were observed on the left and right banks B) Close up of a small-rooted plant growing in the riverbed.

The time frame of the experiment played a key role in the amount of geomorphological evolution that took place. In phase 3, it was possible to detect the beginning of a sinuous curve. However, because of the experiments limited runtime which was constrained due to weather, and costs of running the system, phase 3 was only run for 17 days. The timescales of geomorphological evolution, in particular meanders are difficult to quantify (Hooke, 2007). Small-scaled rivers that experience big events such as flooding often have immediate changes to channel pattern and the

formation of meanders can develop rapidly (Hooke, 2007; Salas and Rhoads, 2022). Other additional elements, including slope, substrate, sinuosity, vegetation and the development of bars also impact the time it takes for meander formation (Hooke, 2007; Braudrick et al., 2009; Kleinham et al., 2009; Salas and Rhoads, 2022). Smaller rivers with higher sediment loads generally develop meanders at a faster rate, while larger rivers with smaller sediment loads take a longer amount of time (Hooke, 2007). The formation of meanders can be highly determinant on pre-existing factors, and it is difficult to quantify the exact timeframe at which meanders will form. At the OERF, the installation of a bar perturbation was an attempt to speed up the geomorphological changes. However, in combination with the conditions previously discussed the runtime was perhaps not sufficient to have significant geomorphological change.

The OERF did not have an influx of continuous sediment supply, and in the absence of this, as the OERF armoured, and sediment transport and morphological changes became limited. The development of bar growth is greatly related to and dependent on the upstream sediment influx (Braudrick et al., 2009). For example, in Braudrick et al. (2009)'s small-scale flume study, for rapid bar development to occur, fine sediments were needed. This is because the fine sediments filled in the voids of the coarser material and enabled the growth of the bars (Braudrick et al., 2009). Their study found that when the banks were strengthened with alfalfa, the channel migrated downstream and developed bars in a small-scale flume (D_{50} = 0.8 mm). Similarly, Van Dijk et al. (2013) found that the sedimentation of fine cohesive sediments on the floodplain were a necessary condition to stimulate meanders because the channel experienced fewer cutoffs. Without these cohesive fines the river generally formed a braided pattern (Van Dijk et al., 2013). Tal and Paola (2010) found that the most likely reasons for the lack of true meander formation was that sediment supply was not adapted to the rate of transport. Therefore, it is likely that since the OERF showed signs of armouring it had limited bar formation because sediment was not constantly entering the system.

Furthering this, in gravel bed rivers, without the addition of sediments, there is a downstream winnowing effect where the surface size is truncated and preferential fractions are removed (Whiting and King, 2023). This was seen at the OERF where the bed armoured and the D_{50} changed from 10 mm to 23 mm following phase 3. Without the addition of new sediments, the river is "supply-limited" (Whiting and King, 2003), and as such bar development and meandering

formation will also be limited (Braudrick et al., 2009; Van Dijk et al., 2013). Armouring of the bed, coupled with the factors already mentioned, such as, limited timescales and too large sediments for the flow rate will reduce the geomorphological changes that can occur to the OERF.

8 Conclusion

Although large geomorphological planform evolution of the OERF did not occur, results of the initial experiments conducted at this new facility provided valuable findings that will be helpful for planning future experiments. Data from the velocity measurement showed that when the perturbation phases were added, there was an overall local velocity increase at the perturbation sites. As the phases progressed, the vectors became increasingly angled towards the banks. At these locations, there was evidence of increased erosion on the banks, which was also observed using the DEMs and through visual observations. In phases 2 and 3, the DEMs showed the most pronounced bank erosion in the area opposing the perturbation. The start of the formation of sinuous curves could be observed by increased erosion on opposite banks. However, the study did not establish the length of time required for the development of meanders or substantial geomorphological changes. It is suggested that in order to speed up morphological change, stronger flows, sediment feed and/or smaller sediment sizes are needed.

The estimation of bank shear stress proved complex even in the relatively simple channel of the OERF, which highlights how challenging quantifying this variable can be in a natural context. Additional research is required to better understand bank shear stress and to determine a robust sampling technique.

This study provides initial insights into the operation of the outdoor experimental river and will pave the way for further initiatives that would deepen our understanding of fluvial processes. With evidence of a changing climate and an increase in flooding incidents, the projects relevance to sustainable river management becomes paramount. The future experiments at the OERF will be instrumental in learning more about rivers at larger scales.

References

Anderson, E. P., Jackson, S., Tharme, R. E., Douglas, M., Flotemersch, J. E., Zwarteveen, M., Lokgariwar, C., Montoya, M., Wali, A., Tipa, G. T., Jardine, T. D., Olden, J. D., Cheng, L., Conallin, J., Cosens, B., Dickens, C., Garrick, D., Groenfeldt, D., Kabogo, J., Arthington, A. H. (2019). Understanding rivers and their social relations: A critical step to advance environmental water management. *WIREs. Water*, *6*(6), 10.1002.

Babaeyan-Koopaei, K., Ervine, D. A., Carling, P. A., & Cao, Z. (2002). Velocity and Turbulence Measurements for Two Overbank Flow Events in River Severn. *Journal of Hydraulic Engineering,* 128(10), 891–900.

Bagnold, R. A. (1966). An approach to the sediment transport problem from general physics (Report No. 422I; Professional Paper). *USGS Publications Warehouse.*

Biedenharn, D. S., Hubbard, L. C., Thorne, C. R., & Watson, C. C. (2006). Understanding Sediment Sources, Pathways, and Sinks in Regional Sediment Management: Application of Wash Load and Bed-Material Load Concept.

Biron, P. M., Robson, C., Lapointe, M. F., & Gaskin, S. J. (2004). Comparing different methods of bed shear stress estimates in simple and complex flow fields. *Earth Surface Processes and Landforms*, 29(11), 1403–1415.

Biron, P. M., Lane, S. N., Roy, A. G., Bradbrook, K. F., & Richards, K. S. (1998). Sensitivity of bed shear stress estimated from vertical velocity profiles: The problem of sampling resolution. *Earth Surface Processes and Landforms*, 23(2), 133–139.

Blanckaert, K., Duarte, A., Chen, Q., & Schleiss, A. J. (2012). Flow processes near smooth and rough (concave) outer banks in curved open channels. *Journal of Geophysical Research: Earth Surface*, 117(F4).

Blondeaux, P., & Seminara, G. (1985). A unified bar–bend theory of river meanders. *Journal of Fluid Mechanics*, 157, 449–470.

Braudrick, C., Dietrich, W., Leverich, G., & Sklar, L. (2009). Experimental Evidence for the Conditions Necessary to Sustain Meandering in Coarse-Bedded Rivers. *Proceedings of the National Academy of Sciences of the United States of America,* 106, 16936–16941.

Bravard, J.P., Amoros, C., & Pautou, G. (1986). Impact of Civil Engineering Works on the Successions of Communities in a Fluvial System: A Methodological and Predictive Approach Applied to a Section of the Upper Rhône River, France. *Oikos*, *47*(1), 92–111.

Brock, B. E., Martin, M. E., Mongeon, C. L., Sokal, M. A., Wesche, S. D., Armitage, D., Wolfe, B. B., Hall, R. I., & Edwards, T. W. D. (2010). Flood Frequency Variability During the Past 80 Years in the Slave River Delta, NWT, as Determined from Multi-Proxy Paleolimnological Analysis. *Canadian Water Resources Journal*, *35*(3), 281–300.

Brown, G. L. (2008). Approximate Profile for Nonequilibrium Suspended Sediment. *Journal of Hydraulic Engineering,* 134(7), 1010–1014 (2008)134:7(1010).

Buffin-Bélanger, T., & Roy, A. G. (1998). Effects of a pebble cluster on the turbulent structure of a depth-limited flow in a gravel-bed river. *Geomorphology*, *25*(3), 249–267.

Bureaus of Reclamation's Water Resources Research Laboratory (1996) WinADV. Technical Service Centre. Retrieved from https://www.usbr.gov/tsc/techreferences/computer%20software/software/winadv/index.html

Carrivick, J. L., & Smith, M. W. (2019). Fluvial and aquatic applications of Structure from Motion photogrammetry and unmanned aerial vehicle/drone technology. WIREs *Water,* 6(1), e1328.

Carson, M.A., 1984, The meandering-braided river threshold: A reappraisal, *Journal of Hydrology*, 73, 315-34.

Cecchetto, M., Tregnaghi, M., Bottacin-Busolin, A., Tait, S. J., Cotterle, L., & Marion, A. (2018). Diffusive Regimes of the Motion of Bed Load Particles in Open Channel Flows at Low Transport Stages. *Water Resources Research*, 54(11), 8674–8691.

Chang, H. H. (1984). Analysis of River Meanders. *Journal of Hydraulic Engineering*, 110(1), 37–50:1(37).

Choné, G., & Biron, P. M. (2016). Assessing the Relationship Between River Mobility and Habitat. *River Research and Applications,* 32(4), 528–539.

Chow, V. T. (1959). Open-channel Hydraulics. Blackburn Press. University of Illinois, 680 pages.

Church, M., 2002, Geomorphic thresholds in riverine landscapes, *Freshwater Biology,* 47, 541-57.

Darby, S. E., Gessler, D., & Thorne, C. R. (2000). Computer program for stability analysis of steep, cohesive riverbanks. *Earth Surface Processes and Landforms*, *25*(2), 175–190.

Dey, S. (2014). Turbulence in Open-Channel Flows. In S. Dey (Ed.), *Fluvial Hydrodynamics: Hydrodynamic and Sediment Transport Phenomena* (pp. 95–187). Springer.

Duan, J. G. (2005). Analytical Approach to Calculate Rate of Bank Erosion. *Journal of Hydraulic Engineering,* 131(11), 980–990 (2005)131:11(980).

Doroudian, B., Bagherimiyab, F., & Lemmin, U. (2010). Improving the accuracy of four-receiver acoustic Doppler velocimeter (ADV) measurements in turbulent boundary layer flows. *Limnology and Oceanography: Methods*, 8(11), 575–591.

Eaton, B. C., Church, M., & Davies, T. R. H. (2006). A conceptual model for meander initiation in bedload-dominated streams. *Earth Surface Processes and Landforms*, 31(7), 875–891.

Engel, F. L., & Rhoads, B. L. (2012). Interaction among mean flow, turbulence, bed morphology, bank failures and channel planform in an evolving compound meander loop. *Geomorphology*, 163, 70-83.

Engel, F. L., & Rhoads, B. L. (2017). Velocity profiles and the structure of turbulence at the outer bank of a compound meander bend. *Geomorphology*, 295, 191–201.

Famiglietti, J.S. 2014. The global groundwater crisis. *Nature Climate Change*. 4(11):945-948.

Fang, Y., Ceola, S., Paik, K., McGrath, G., Rao, P. S. C., Montanari, A., & Jawitz, J. W. (2018). Globally Universal Fractal Pattern of Human Settlements in River Networks. *Earth's Future,* 6(8), 1134–1145.

Ferguson, R.I. 1987, Hydraulic and sedimentary controls of channel pattern, in *River Channels: Environment and Process*, Blackwell: Oxford, 129-58.

Florsheim JL, Mount JF, Chin A. (2008). Bank erosion as a desirable attributes of rivers. *Bioscience*, 58 : 519–529.

Friedkin, J.F., 1945. A laboratory study of the meandering of alluvial rivers. *U.S. Waterways Experiment Station, Vicksburg*, MS, 40 pp.

Goharrokhi, M. (2015). Effect of Hydraulic Shear Stress on the Banks of the Red River. *Masters Thesis, University of Manitoba.* 1- 153.

Gori, A., Lin, N., Xi, D., Emanuel, K. (2022) Tropical cyclone climatology change greatly exacerbates US extreme rainfall–surge hazard. *Nature Climate Change*, 12: 171-178.

Guo, J., & Zhang, J. (2016). Velocity distributions in laminar and turbulent vegetated flows. *Journal of Hydraulic Research*, 54(2), 117–130.

He, L. (2018). Distribution of primary and secondary currents in sine-generated bends. *Water SA,* 44(1), Article 1.

Hooke, R. L. B. (1975). Distribution of Sediment Transport and Shear Stress in a Meander Bend. *The Journal of Geology*, 83(5), 543–565.

Hopkinson, L. C., & Wynn-Thompson, T. M. (2016). Comparison of Direct and Indirect Boundary Shear Stress Measurements along Vegetated Streambanks. *River Research and Applications,* 32(8), 1755–1764.

Hupp, C. R., & Osterkamp, W. R. (1996). Riparian vegetation and fluvial geomorphic processes. *Geomorphology*, 14(4), 277–295.

Kang, S., & Sotiropoulos, F. (2011). Flow phenomena and mechanisms in a field-scale experimental meandering channel with a pool-riffle sequence: Insights gained via numerical simulation. *Journal of Geophysical Research: Earth Surface*, *116*(F3).

Kim, S. C., Friedrichs, C.T., Maa, J. P.Y., and Wright, L. D. (2000). "Estimating bottom stress in tidal boundary layer from acoustic Doppler velocimeter data." *J. Hydraul. Eng.,* 126(6), 399–406.

Kleinhans, M. G., Schuurman, F., Bakx, W., & Markies, H. (2009). Meandering channel dynamics in highly cohesive sediment on an intertidal mud flat in the Westerschelde estuary, the Netherlands. *Geomorphology,* 105(3), 261–276.

Knighton, David (1998) Fluvial Forms & Processes. A New Perspective. Don Mills, Ontario, Oxford University Press, 383 p.

Kozarek, J. L., Limaye, A. B., & Arpin, E. (2023). Comparing turbulent flow and bank erosion with controlled experiments in a field-scale meandering channel. *Geological Society*, London, Special Publications, 540(1), SP540-2023–17.

Lane, S. N., Biron, P. M., Bradbrook, K. F., Butler, J. B., Chandler, J. H., Crowell, M. D., McLelland, S. J., Richards, K. S., & Roy, A. G. (1998). Three-dimensional measurement of river channel flow processes using acoustic doppler velocimetry. *Earth Surface Processes and Landforms*, 23(13), 1247–1267.

Leopold, L. B., & Wolman, M. G. (1957). River Channel Patterns: Braided, Meandering, and Straight. U.S. Government Printing Office.

Lewin, J. (1976). Initiation of bed forms and meanders in coarse-grained sediment. *GSA Bulletin,* 87(2), 281–285.

Leyland, J., Hackney, C. R., Darby, S. E., Parsons, D. R., Best, J. L., Nicholas, A. P., Aalto, R., & Lague, D. (2017). Extreme flood-driven fluvial bank erosion and sediment loads: Direct process measurements using integrated Mobile Laser Scanning (MLS) and hydro-acoustic techniques. *Earth Surface Processes and Landforms,* 42(2), 334–346.

Li, X., Zhang, L., & Zhang, Z. (2006). Soil bioengineering and the ecological restoration of riverbanks at the Airport Town, Shanghai, China. *Ecological Engineering*, *26*(3), 304–314.

Lin, Y.-T., Yang, Y., Chiu, Y.-J., & Ji, X. (2021). Hydrodynamic Characteristics of Flow in a Strongly Curved Channel with Gravel Beds. *Water,* 13(11), Article 11.

Liu, Y., Stoesser, T., Fang, H., Papanicolaou, A., & Tsakiris, A. G. (2017a). Turbulent flow over an array of boulders placed on a rough, permeable bed. *Computers & Fluids*, 158, 120–132.

Liu, D., Valyrakis, M., & Williams, R. (2017b). Flow Hydrodynamics across Open Channel Flows with Riparian Zones: Implications for Riverbank Stability. *Water*, *9*(9), 720.

Lucking, G., Stark, N., Lippmann, T., & Smyth, S. (2017). Variability of in situ sediment strength and pore pressure behavior of tidal estuary surface sediments. *Geo-Marine Letters,* 37(5), 441–456.

Maciel-Pearson, B. G., Akcay, S., Atapour-Abarghouei, A., Holder, C., & Breckon, T. P. (2019). Multi-Task Regression-based Learning for Autonomous Unmanned Aerial Vehicle Flight Control within Unstructured Outdoor Environments. *IEEE Robotics and Automation Letters*, 1-8.

Mahmoud, B (Research Partner-OERF) (2022a). *Drawing of River* Perturbation: A, Université de Sherbrooke.

Mahmoud, B. (2022b) Impacts of riverbank erosion and stabilization planform change and flow structure. University of Sherbrooke, DPR.

Macklin, M. G., & Lewin, J. (2019). River stresses in anthropogenic times: Large-scale global patterns and extended environmental timelines. *Progress in Physical Geography: Earth and Environment,* 43(1), 3–23.

Marren, P. M., Grove, J. R., Webb, J. A., & Stewardson, M. J. (2014). The Potential for Dams to Impact Lowland Meandering River Floodplain Geomorphology. *The Scientific World Journal*, 2014, e309673.

Martin, V., Fisher, T. S. R., Millar, R. G., & Quick, M. C. (2012). *ADV Data Analysis for Turbulent Flows: Low Correlation Problem*. 1–10.

Nardi, L., Campo, L., & Rinaldi, M. (2013a). Quantification of riverbank erosion and application in risk analysis. *Natural Hazards*, *69*(1), 869–887.

Nicholas, A. p. (2000). Computational fluid dynamics modelling of boundary roughness in gravel-bed rivers: An investigation of the effects of random variability in bed elevation. *Earth Surface Processes and Landforms,* 26(4), 345–362.

Nikora, V., & Goring, D. (2000). Flow Turbulence over Fixed and Weakly Mobile Gravel Beds. *Journal of Hydraulic Engineering*, 126(9), 679–690.

Osman, A. M., and C. R. Thorne. 1988. Riverbank stability analysis I: Theory. *Journal of Hydraulic Engineering.* 114: 134-150.

Öztürk, M. (2017). Sediment Size Effects in Acoustic Doppler Velocimeter-Derived Estimates of Suspended Sediment Concentration. *Water,* 9(7), Article 7.

Palmsten, M. L., Kozarek, J. L., & Calantoni, J. (2015). Video observations of bed form morphodynamics in a meander bend. *Water Resources Research*, 51(9), 7238–7257.

Panagoulia, D., & Dimou, G. (1997). Sensitivity of flood events to global climate change. *Journal of Hydrology*, *191*(1–4), 208–222.

Parker, G., & Klingeman, P. C. (1982). On why gravel bed streams are paved. *Water Resources Research,* 18(5), 1409–1423.

Parker, G., Shimizu, Y., Wilkerson, G. V., Eke, E. C., Abad, J. D., Lauer, J. W., Paola, C., Dietrich, W. E., & Voller, V. R. (2011). A new framework for modeling the migration of meandering rivers. *Earth Surface Processes and Landforms,* 36(1), 70–86.

Partheniades, E. (1965). Erosion and Deposition of Cohesive Soils. *Journal of the Hydraulics Division,* 91(1), 105–139.

Peakall, J., Ashworth, P., Best, J.L. (1996) Physical modelling in fluvial geomorphology: Principles, applications and unresolved issues. In: *The Scientific Nature of Geomorphology: Proceedings of the 27th Binghamton Symposium in Geomorphology*, Rhoads, B.L., Thorn, C.E. (Eds), Wiley & Sons, 221-253.

Piégay, H., Cuaz, M., Javelle, E., & Mandier, P. (1997). Bank erosion management based on geomorphological, ecological and economic criteria on the Galaure River, France. *Regulated Rivers: Research & Management*, *13*(5), 433–448.

Pirkhoffer, E., Halmai, Á., Ficsor, J., Gradwohl-Valkay, A., Lóczy, D., Nagy, Á., Liptay, Z. Á., & Czigány, S. (2021). Bedload entrainment dynamics in a partially channelized river with mixed

bedload: A case study of the Drava River, Hungary. *River Research and Applications*, *37*(5), 699–711.

Pradhan, A., Kumar Khatua, K., & Sankalp, S. (2018). Variation of Velocity Distribution in Rough Meandering Channels. *Advances in Civil Engineering*, 2018, e1569271.

Reid, D., & Church, M. (2015a). Geomorphic and Ecological Consequences of Riprap Placement in River Systems. *JAWRA Journal of the American Water Resources Association*, *51.*

Redolfi, M., Welber, M., Carlin, M., Tubino, M., & Bertoldi, W. (2020). Morphometric properties of alternate bars and water discharge: A laboratory investigation. *Earth Surface Dynamics*, 8(3), 789–808.

Rehmel, M. (2007). Application of Acoustic Doppler Velocimeters for Streamflow Measurements. *Journal of Hydraulic Engineering*, 133(12), 1433–1438.

Renault, A. (Research Partner-OERF) (2021). *AutoCAD Drawing of River*. Université de Sherbrooke.

Renault, A. (Research Partner-OERF) (2023). *AutoCAD Drawing of River ADV Points*. Université de Sherbrooke.

Rey, F. (2009). A strategy for fine sediment retention with bioengineering works in eroded marly catchments in a mountainous Mediterranean climate (Southern ALPS, France). *Land Degradation & Development*, 20(2), 210–216.

Rhoads, B. L., & Welford, M. R. (1991). Initiation of river meandering. *Progress in Physical Geography: Earth and Environment,* 15(2), 127–156.

Riesterer, J., Wenka, T., Brudy-Zippelius, T., & Nestmann, F. (2016). Bed load transport modeling of a secondary flow influenced curved channel with 2D and 3D numerical models. *Journal of Applied Water Engineering and Research*, 4(1), 54–66.

Rinaldi, M., & Darby, S. E. (2007). 9 Modelling river-bank-erosion processes and mass failure mechanisms: Progress towards fully coupled simulations. In H. Habersack, H. Piégay, & M. Rinaldi (Eds.), *Developments in Earth Surface Processes* (Vol. 11, pp. 213–239). Elsevier.

Rodriguez-Iturbe, I., Muneepeerakul, R., Bertuzzo, E., Levin, S. A., & Rinaldo, A. (2009). River networks as ecological corridors: A complex systems perspective for integrating hydrologic, geomorphologic, and ecologic dynamics. *Water Resources Research,* 45(1).

Rüther, N., & Olsen, N. R. B. (2007). Modelling free-forming meander evolution in a laboratory channel using three-dimensional computational fluid dynamics. *Geomorphology*, 89(3–4), 308–319.

Sahagian, D., Diplas, P., Urban, C., Cheng, Z., & David, M. (2022). In search of a unifying criterion for meandering systems: Examples from natural and built environments. *Environmental Fluid Mechanics*, 1–28.

Salas, C. R., & Rhoads, B. L. (2022). Big Pine Creek Ditch revisited: Planform recovery to channelization and the timescale of river meandering. *Geomorphology*, 403, 108140.

Schwartz, J. S., Neff, K. J., Dworak, F. E., & Woockman, R. R. (2015). Restoring riffle-pool structure in an incised, straightened urban stream channel using an ecohydraulic modeling approach. *Ecological Engineering,* 78, 112–126.

Semmad, S., Jotisankasa, A., Mahannopkul, K., & Inazumi, S. (2021). A coupled simulation of lateral erosion, unsaturated seepage and bank instability due to prolonged high flow. *Geomechanics for Energy and the Environment*, 100301.

Schumm, S. A., & Khan, H. R. (1971). Experimental Study of Channel Patterns. *Nature*, 233(5319), 407–409.

Schuurman, F., Shimizu, Y., Iwasaki, T., & Kleinhans, M. G. (2016). Dynamic meandering in response to upstream perturbations and floodplain formation. *Geomorphology*, 253, 94–109.

Sieben, J. (1999). A theoretical analysis on armouring of river beds. Une analyse théorique du pavage du lit des rivières. *Journal of Hydraulic Research*, *37*(3), 313–326.

Siegel and Castellan (1988) Non parametric statistics for the behavioural sciences. *MacGraw Hill Int.,* New York. pp 213-214.

Sin, K-S., Thornton, C.I., Cox, A.L., and Abt, S.R. (2012). Methodology for calculating shear stress in a meandering channel. *Colardao State University: Prepared for U.S. Department of the Interior.* 1-168.

Smart, G. M. (1999). Turbulent Velocity Profiles and Boundary Shear in Gravel Bed Rivers. *Journal of Hydraulic Engineering*, 125(2), 106–116.

Stoesser, T., Ruether, N., & Olsen, N. R. B. (2010). Calculation of primary and secondary flow and boundary shear stresses in a meandering channel. *Advances in Water Resources*, 33(2), 158–170.

Tabari, H. (2020). Climate change impact on flood and extreme precipitation increases with water availability. *Scientific Reports*, *10*(1), 13768.

Tal, M., & Paola, C. (2010). Effects of vegetation on channel morphodynamics: Results and insights from laboratory experiments. *Earth Surface Processes and Landforms,* 35(9), 1014–1028.

Talbot, C. J., Bennett, E. M., Cassell, K., Hanes, D. M., Minor, E. C., Paerl, H., Raymond, P. A., Vargas, R., Vidon, P. G., Wollheim, W., & Xenopoulos, M. A. (2018). The impact of flooding on aquatic ecosystem services. *Biogeochemistry*, *141*(3), 439–461.

Tani, I. (1977). History of Boundary Layer Theory. *Annual Review of Fluid Mechanics*, 9(1), 87–111.

Thorne, C. R., & Tovey, N. K. (1981). Stability of composite river banks. *Earth Surface Processes and Landforms*, 6(5), 469–484.

Tokyay, T., & Sinha, S. (2020). Channel width, bedform length and turbulence: Numerical investigation of flow dynamics over laboratory-scale pool–riffle sequences. *Environmental Fluid Mechanics,* 20(4), 819–842.

Turowski, J. M., Wyss, C. R., & Beer, A. R. (2015). Grain size effects on energy delivery to the streambed and links to bedrock erosion. *Geophysical Research Letters*, 42(6), 1775–1780.

United States Environmental Protection Agency (2003). Sediments. *Caddis Volume 2.* Retrieved March 23, 2023 from https://www.epa.gov/caddis-vol2/sediments.

van Dijk, W. M., van de Lageweg, W. I., & Kleinhans, M. G. (2012). Experimental meandering river with chute cutoffs. *Journal of Geophysical Research: Earth Surface,* 117(F3).

van Dijk, W. M., van de Lageweg, W. I., & Kleinhans, M. G. (2013). Formation of a cohesive floodplain in a dynamic experimental meandering river. *Earth Surface Processes and Landforms*, 38(13), 1550–1565.

Van Rijn, V., & C, L. (1984). Sediment Transport, Part I: Bed Load Transport. *Journal of Hydraulic Engineering,* 110(10), 1431–1456.

Vargas-Luna, A., Duró, G., Crosato, A., & Uijttewaal, W. (2019). Morphological Adaptation of River Channels to Vegetation Establishment: A Laboratory Study. *Journal of Geophysical Research: Earth Surface,* 124(7), 1981–1995.

Wahl, T. L. (2012). Analyzing ADV Data Using WinADV. 1–10.

Weisscher, S. A. H., Shimizu, Y., & Kleinhans, M. G. (2019). Upstream perturbation and floodplain formation effects on chute-cutoff-dominated meandering river pattern and dynamics. *Earth Surface Processes and Landforms,* 44(11), 2156–2169.

Werner, P.W. (1951). On the Origin of River Meanders. *Transactions, American Geophysical Union.* 32 (6): 898-902.

Whiting, P. J., & King, J. G. (2003). Surface particle sizes on armoured gravel streambeds: Effects of supply and hydraulics. *Earth Surface Processes and Landforms,* 28(13), 1459–1471.

Wijesekara, G., Gupta, A., Valeo, C., Hasbani, J.G., Qiao, Y., Delaney, P., & Marceau, D. (2012). Assessing the Impact of Future Land-Use Changes on Hydrological Processes in the Elbow River Watershed in Southern Alberta, Canada. *Journal of Hydrology*, *412*, 220–232.

Wilcock, P., & Crowe, J. (2003). Surface-based Transport Model for Mixed-Size Sediment. *Journal of Hydraulic Engineering-Asce - J HYDRAUL ENG-ASCE*, 129.

Wilcock, P. R., Orr, C. H., & Marr, J. D. G. (2008). The Need for Full-Scale Experiments in River Science. Eos, *Transactions American Geophysical Union*, 89(1), 6–6.

Williams JJ. 1995. Drag and sediment dispersion over sand waves. *Estuarine, Coastal and Shelf Science* 41: 659–687.

Woodget, A. S., & Austrums, R. (2017a). Subaerial gravel size measurement using topographic data derived from a UAV-SfM approach. *Earth Surface Processes and Landforms*, *42*(9), 1434–1443.

Woodget, A. S., Austrums, R., Maddock, I. P., & Habit, E. (2017b). Drones and digital photogrammetry: From classifications to continuums for monitoring river habitat and hydromorphology. *WIREs Water*, *4*(4), e1222.

Woodget, A. S., Fyffe, C., & Carbonneau, P. E. (2018). From manned to unmanned aircraft: Adapting airborne particle size mapping methodologies to the characteristics of sUAS and SfM. *Earth Surface Processes and Landforms*, *43*(4), 857–870.

Yu, M., Wei, H., & Wu, S. (2015). Experimental study on the bank erosion and interaction with near-bank bed evolution due to fluvial hydraulic force. *International Journal of Sediment Research*, 30(1), 81–89.

Zolezzi, G., & Seminara, G. (2001). Downstream and upstream influence in river meandering. Part 1. General theory and application to overdeepening. *Journal of Fluid Mechanics.*